[19,31] and TGF-β3 [19,30,31,33,34] also play important roles in the process of fibrotic scar formation, although their relative dominance during scar development is smaller when compared with TGF-β1 and CTGF, and their effects on scarring were not clearly defined as pro- or antifibrotic. On the other hand, HGF is reported to have antifibrogenic effects in various organs [35,36], and much more recently, bFGF was found to prevent fibrogenesis via activation of HGF secretion from adipose-derived cells and dermal fibroblasts [37]. Therefore, we also investigated the expression of HGF and bFGF as possible antifibrotic factors.

Between facial and trunk dermal fibroblasts, differences in expression and/or production of fibrosis-associated factors have been noted. In particular, it was noted that expression and production of TGF-β1 and CTGF, known as one of the most potent fibrosis-inducing factors [6,12,24,30,32], were lower in facial fibroblasts than in trunk fibroblasts. Moreover, with regard to superficial dermal fibroblasts, facial fibroblasts showed lower expression and/or production of ECMs than trunk fibroblasts. This indicates that facial dermal fibroblasts are intrinsically less fibrotic than trunk dermal fibroblasts, although the reasons for the differences in TGF-β2 and TGF-β3 expressions in fibrosis are unclear.

Our study demonstrated that facial and trunk dermal fibroblasts in the superficial and deep dermis possess identical proliferative capacity, but that facial dermal fibroblasts show lower fibrotic activity in mRNA expression and protein production analyses. We believe that these functional differences in local dermal fibroblasts are at least partly responsible for the clinically observed differences in scarring in the face and trunk. (Facial wounds tend to heal with less scarring than trunk wounds.)

As noted by Chang et al. in a genome-wide mRNA expression analysis using a microarray, fibroblasts obtained from various body sites displayed distinct and characteristic transcriptional patterns, particularly with regard to HOX genes established during embryogenesis, and fibroblasts at different locations in the body should be considered as distinct differentiated cell types [16]. During the developmental process, the dermal component is generally derived from lateral plate mesoderm and somite [38], however, the dermis of the face and ventral neck area is specifically differentiated from neural crest cells via formation of mesoectoderm [38,39]. We believe that these developmental differences are the cause of the functional differences observed in our study. Future studies should aim to clarify more fundamental differences between facial and dermal fibroblasts, similar to the work of Yamaguchi et al., which revealed that the physiological differences in melanin pigment between palmoplantar and nonpalmoplantar skin are associated with elevated expression of dickkopf-1, an inhibitor of the canonical Wnt signaling pathway which is also associated with developmental processes [18]. Further clarification of key factors in the anatomical differences in the scarring properties of fibroblasts may contribute to future therapeutic intervention for problematic wound scarring, such as conspicuous scars resulting from excess scar formation, hypertrophic scarring, or keloids.

Conclusions

Our study demonstrated that facial and trunk dermal fibroblasts in the superficial and deep dermis possess identical proliferative capacity, but that facial dermal fibroblasts show lower fibrotic activity in mRNA expression and protein production analyses. The differences in functional properties of facial and trunk dermal fibroblasts were consistent with the clinical healing tendencies of facial and trunk wounds. Thus, the differences between facial and trunk scarring are, in part, related to the intrinsic nature of the local dermal fibroblasts.

Acknowledgment

This work was supported by a grant from the Japanese Ministry of Education, Culture, Sports, Science, and Technology (MEXT) KAKENHI 21689046 (Grant-in-Aid for Young Scientists A) and 20390457 (Grant-in-Aid for Scientific Research B).

Declaration of interest

The authors declare that they have no other competing financial interests.

References

1. Martin, P. (1997). Wound healing – Aiming for perfect skin regeneration. *Science.* 276:75–81.
2. Fries, K.M., Blieden, T., Looney, R.J., Sempowski, G.D., Silvera, M.R., Willis, R.A., and Phipps, R.P. (1994). Evidence of fibroblast heterogeneity and the role of fibroblast subpopulations in fibrosis. *Clin. Immunol. Immunopathol.* 72:283–292.
3. Sorrell, J.M., and Caplan, A.I. (2004). Fibroblast heterogeneity: More than skin deep. *J. Cell Sci.* 117:667–675.
4. Sorrell, J.M., Baber, M.A., and Caplan, A.I. (2004). Site-matched papillary and reticular human dermal fibroblasts differ in their release of specific growth factors/cytokines and in their interaction with keratinocytes. *J. Cell. Physiol.* 200:134–145.
5. Sorrell, J.M., Baber, M.A., and Caplan, A.I. (2008). Human dermal fibroblast subpopulations; differential interactions with vascular endothelial cells in coculture: Nonsoluble factors in the extracellular matrix influence interactions. *Wound Repair Regen.* 16:300–309.
6. Smith, J.C., Boone, B.E., Opalenik, S.R., Williams, S.M., and Russell, S.B. (2008). Gene profiling of keloid fibroblasts shows altered expression in multiple fibrosis-associated pathways. *J. Invest. Dermatol.* 128: 1298–1310.
7. Dasu, M.R., Hawkins, H.K., Barrow, R.E., Xue, H., and Herndon, D.N. (2004). Gene expression profiles from hypertrophic scar fibroblasts before and after IL-6 stimulation. *J. Pathol.* 202:476–485.
8. Jelaska, A., Arakawa, M., Broketa, G., and Korn, J.H. (1996). Heterogeneity of collagen synthesis in normal and systemic sclerosis skin fibroblasts. Increased proportion of high collagen-producing cells in systemic sclerosis fibroblasts. *Arthritis Rheum.* 39:1338–1346.
9. De Schepper, S., Boucneau, J., Vander Haeghen, Y., Messiaen, L., Naeyaert, J.M., and Lambert, J. (2006). Café-au-lait spots in neurofibromatosis type 1 and in healthy control individuals: Hyperpigmentation of a different kind? *Arch. Dermatol. Res.* 297:439–449.
10. Okazaki, M., Yoshimura, K., Suzuki, Y., Uchida, G., Kitano, Y., Harii, K., and Imokawa, G. (2003). The mechanism of epidermal hyperpigmentation in café-au-lait macules of neurofibromatosis type 1 (von Recklinghausen's disease) may be associated with dermal fibroblast-derived stem cell factor and hepatocyte growth factor. *Br. J. Dermatol.* 148:689–697.
11. Ali-Bahar, M., Bauer, B., Tredget, E.E., and Ghahary, A. (2004). Dermal fibroblasts from different layers of human skin are heterogeneous in expression of collagenase and types I and III procollagen mRNA. *Wound Repair Regen.* 12:175–182.
12. Wang, J., Dodd, C., Shankowsky, H.A., Scott, P.G., Tredget, E.E., and Wound Healing Research Group. (2008). Deep dermal fibroblasts contribute to hypertrophic scarring. *Lab. Invest.* 88:1278–1290.
13. Harper, R.A., and Grove, G. (1979). Human skin fibroblasts derived from papillary and reticular dermis: Differences in growth potential in vitro. *Science* 204:526–527.
14. Azzarone, B., and Macieira-Coelho, A. (1982). Heterogeneity of the kinetics of proliferation within human skin fibroblastic cell populations. *J. Cell. Sci* 57:177–187.
15. Schafer, I.A., Pandy, M., Ferguson, R., and Davis, B.R. (1985). Comparative observation of fibroblasts derived from the papillary and reticular dermis of infants and adults: Growth kinetics, packing density ant confluence and surface morphology. *Mech. Ageing Dev.* 31:275–293.
16. Chang, H.Y., Chi, J.T., Dudoit, S., Bondre, C., van de Rijn, M., Botstein, D., and Brown, P.O. (2002). Diversity, topographic differentiation, and positional memory in human fibroblasts. *Proc. Natl. Acad. Sci. USA* 99 (20):12877–12882.

17. Rinn, J.L., Bondre, C., Gladstone, H.B., Brown, P.O., and Chang, H.Y. (2006). Anatomic demarcation by positional variation in fibroblast gene expression programs. *PLoS Genet.* 2:e119.
18. Yamaguchi, Y., Passeron, T., Watabe, H., Yasumoto, K., Rouzaud, F., Hoashi, T., and Hearing, V.J. (2007). The effects of dickkopf 1 on gene expression and Wnt signaling by melanocytes: Mechanisms underlying its suppression of melanocyte function and proliferation. *J. Invest. Dermatol.* 127:1217–1225.
19. Ferguson, M.W., and O'Kane, S. (2004). Scar-free healing: From embryonic mechanisms to adult therapeutic intervention. *Philos. Trans. R. Soc. Lond. B Biol. Sci.* 359:839–850.
20. Gangemi, E.N., Gregori, D., Berchialla, P., Zingarelli, E., Cairo, M., Bollero, D., Ganem, J., Capocelli, R., Cuccuru, F., Cassano, P., Risso, D., and Stella, M. (2008). Epidemiology and risk factors for pathologic scarring after burn wounds. *Arch. Facial. Plast. Surg.* 10:93–102.
21. Thiele, B.J., Doller, A., Kähne, T., Pregla, R., Hetzer, R., and Regitz-Zagrosek, V. (2004). RNA-binding proteins heterogeneous nuclear ribonucleoprotein A1, E1, and K are involved in post-transcriptional control of collagen I and III synthesis. *Circ. Res.* 95:1058–1066.
22. Suga, H., Matsumoto, D., Eto, H., Inoue, K., Aoi, N., Kato, H., Araki, J., and Yoshimura, K. (2009). Functional implications of CD34 expression in human adipose-derived stem/progenitor cells. *Stem Cells Dev.* 18:1201–1210.
23. Goldberg, M.T., Han, Y.P., Yan, C., Shaw, M.C., and Garner, W.L. (2007). TNF-alpha suppresses alpha-smooth muscle actin expression in human dermal fibroblasts: An implication for abnormal wound healing. *J. Invest. Dermatol.* 127:2645–2655.
24. Pohlers, D., Beyer, A., Koczan, D., Wilhelm, T., Thiesen, H.J., and Kinne, R.W. (2007). Constitutive upregulation of the transforming growth factor-beta pathway in rheumatoid arthritis synovial fibroblasts. *Arthritis. Res. Ther.* 9:R59.
25. Quesnel, C., Marchand-Adam, S., Fabre, A., Marchal-Somme, J., Philip, I., Lasocki, S., Leçon, V., Crestani, B., and Dehoux, M. (2008). Regulation of hepatocyte growth factor secretion by fibroblasts in patients with acute lung injury. *Am. J. Physiol. Lung. Cell. Mol. Physiol.* 294:L334–L343.
26. Ala-Kokko, L., Rintala, A., and Savolainen, E.R. (1987). Collagen gene expression in keloid. Analysis of collagen metabolism and type I, III, IV and V procollagen mRNAs in keloid tissue and keloid fibroblast cultures. *J. Invest. Dermatol.* 89:238–244
27. Ghahary, A., Shen, Y.J., Nedelec, B., Wang, R., Scott, P.G., and Tredget, E.E. (1996). Collagenase production is lower in post-burn hypertrophic scar fibroblasts than normal fibroblasts and is down-regulated by insulin-like growth factor-1. *J. Invest. Dermatol.* 106:476–481.
28. Derynck, R., and Zhang, Y.E. (2003). Smad-dependent and Smad-independent pathways in TGF-β family signalling. *Nature* 425: 577–584.
29. Amjad, S.B., Carachi, R., and Edward, M. (2007). Keratinocyte regulation of TGF-beta and connective tissue growth factor expression: A role in suppression of scar tissue formation. *Wound Repair Regen.* 15: 748–755.
30. Barrientos, S., Stojadinovic, O., Golinko, M.S., Brem, H., and Tomic-Canic, M. (2008). Growth factors and cytokines in wound healing. *Wound Repair Regen.* 16:585–601.
31. Shah, M., Foreman, D.M., and Ferguson, M.W. (1995). Neutralisation of TGF-beta 1 and TGF-beta 2 or exogenous addition of TGF-beta 3 to cutaneous rat wounds reduces scarring. *J. Cell. Sci.* 108:985–1002.
32. Frazier, K., Williams, S., Kothapalli, D., Klapper, H., and Grotendorst, G.R. (1996). Stimulation of fibroblast cell growth, matrix production, and granulation tissue formation by connective tissue growth factor. *J. Invest. Dermatol.* 107:404–411.
33. Wu, L., Siddiqui, A., Morris, D.E., Cox, D.A., Roth, S.I., and Mustoe, T.A. (1997). Transforming growth factor beta 3 (TGF beta 3) accelerates wound healing without alteration of scar prominence. Histologic and competitive reverse-transcription polymerase chain reaction studies. *Arch. Surg.* 132:753–760.
34. Murata, H., Zhou, L., Ochoa, S., Hasan, A., Badiavas, E., and Falanga, V. (1997). F-beta3 stimulates and regulates collagen synthesis through TGF-beta1-dependent and independent mechanisms. *J. Invest. Dermatol.* 108:258–262.
35. Ueki, T., Kaneda, Y., Tsutsui, H., Nakanishi, K., Sawa, Y., Morishita, R., Matsumoto, K., Nakamura, T., Takahashi, H., Okamoto, E., and Fujimoto, J. (1999). Hepatocyte growth factor gene therapy of liver cirrhosis in rats. *Nat. Med.* 5:226–230.
36. Liu, Y. (2004). Hepatocyte growth factor in kidney fibrosis: Therapeutic potential and mechanisms of action. *Am. J. Physiol. Renal. Physiol.* 287:7–16.
37. Suga, H., Eto, H., Shigeura, T., Inoue, K., Aoi, N., Kato, H., Nishimura, S., Manabe, I., Gonda, K., and Yoshimura, K. (2009). S collection: Fibroblast growth factor-2-induced hepatocyte growth factor secretion by adipose-derived stromal cells inhibits postinjury fibrogenesis through a c-Jun N-terminal kinase-dependent mechanism. *Stem Cells* 27:238–249.
38. Sadler, T.W. (2009). *Langman's Medical Embryology*, 11th ed. Philadelphia: Lippincott Williams & Wilkins.
39. Nakamura, H. (1982). Mesenchymal derivatives from the neural crest. *Arch. Histol. Jpn.* 45:127–138.

OPEN ACCESS Freely available online

PLoS one

Procyanidin B3 Prevents Articular Cartilage Degeneration and Heterotopic Cartilage Formation in a Mouse Surgical Osteoarthritis Model

Hailati Aini[1], Hiroki Ochi[2], Munetaka Iwata[3], Atsushi Okawa[4], Daisuke Koga[4], Mutsumi Okazaki[1], Atsushi Sano[5], Yoshinori Asou[4]*

1 Department of Plastic and Reconstructive Surgery, Tokyo Medical and Dental University, Tokyo, Japan, 2 Department of Internal Medicine, Keio University, Tokyo, Japan, 3 Division of Veterinary Surgery, School of Veterinary Medicine, Nippon Veterinary and Life Science University, Tokyo, Japan, 4 Department of Orthopedic Surgery, Tokyo Medical and Dental University, Tokyo, Japan, 5 Research and Development Division, Kikkoman Corporation, Chiba, Japan

Abstract

Osteoarthritis (OA) is a common disease in the elderly due to an imbalance in cartilage degradation and synthesis. Heterotopic ossification (HO) occurs when ectopic masses of endochondral bone form within the soft tissues around the joints and is triggered by inflammation of the soft tissues. Procyanidin B3 (B3) is a procyanidin dimer that is widely studied due to its high abundance in the human diet and antioxidant activity. Here, we evaluated the role of B3 isolated from grape seeds in the maintenance of chondrocytes *in vitro* and *in vivo*. We observed that B3 inhibited H_2O_2-induced apoptosis in primary chondrocytes, suppressed H_2O_2- or IL-1ß−induced nitric oxide synthase (iNOS) production, and prevented IL-1ß−induced suppression of chondrocyte differentiation marker gene expression in primary chondrocytes. Moreover, B3 treatment enhanced the early differentiation of ATDC5 cells. To examine whether B3 prevents cartilage destruction *in vivo*, OA was surgically induced in C57BL/6J mice followed by oral administration of B3 or vehicle control. Daily oral B3 administration protected articular cartilage from OA and prevented chondrocyte apoptosis in surgically-induced OA joints. Furthermore, B3 administration prevented heterotopic cartilage formation near the surgical region. iNOS protein expression was enhanced in the synovial tissues and the pseudocapsule around the surgical region in OA mice fed a control diet, but was reduced in mice that received B3. Together, these data indicated that in the OA model, B3 prevented OA progression and heterotopic cartilage formation, at least in a part through the suppression of iNOS. These results support the potential therapeutic benefits of B3 for treatment of human OA and heterotopic ossification.

Citation: Aini H, Ochi H, Iwata M, Okawa A, Koga D, et al. (2012) Procyanidin B3 Prevents Articular Cartilage Degeneration and Heterotopic Cartilage Formation in a Mouse Surgical Osteoarthritis Model. PLoS ONE 7(5): e37728. doi:10.1371/journal.pone.0037728

Editor: Frank Beier, University of Western Ontario, Canada

Received December 23, 2011; **Accepted** April 23, 2012; **Published** May 22, 2012

Funding: This work was supported by Grants-in-Aid for Scientific Research (Grant Number C21591935) from the Japanese Ministry of Education, Culture, Sports, Science and Technology and also by the Kikkoman Corporation. The funders had no role in study design, data collection and analysis, decision to publish, or preparation of the manuscript. No additional external funding was received for this study.

Competing Interests: Atsushi Sano is employed by Kikkoman Corporation as a research scientist of the Research and Development Division. The Kikkoman Corporation is one of the funders of this study. There are no patents, products in development or marketed products to declare. This does not alter the authors' adherence to all the PLoS ONE policies on sharing data and materials, as detailed online in the guide for authors.

* E-mail: aso.orth@tmd.ac.jp

Introduction

Osteoarthritis (OA) is a common disease in the elderly due to an imbalance in cartilage degradation and synthesis. In OA, articular chondrocytes appear to be eliminated by apoptosis [1–3]. The number of apoptotic cells in articular cartilage is significantly higher in OA patients than in healthy subjects. In response to cytokine stimulation, articular chondrocytes can produce a variety of reactive oxygen species (ROS), including peroxynitrite, superoxide anions, nitric oxide (NO), and hydrogen peroxide (H_2O_2) [4–6]. IL-1β induces chondrocyte death only when used in combination with oxygen radical scavengers or with a CD95 agonist [7,8]. The apoptosis-enhancing pathway induced by IL-1β depends on the generation of ROS [8]. Primary OA chondrocytes show both spontaneous and inducible levels of lipid peroxidation activity [9]. Thus, ROS are among the key inflammatory mediators involved in chondrocyte apoptosis observed in OA. H_2O_2 induces apoptosis in many cell types and may mediate cartilage degeneration associated with inflammatory joint diseases that induce chondrocyte apoptosis [10,11].

NO has been increasingly recognized as a signaling intermediate of IL-1−induced responses in many cell types [4,12], including chondrocytes [13,14]. NO also regulates aggrecanase activity and induces aggrecan degeneration in chondrocytes [15]. Endogenously synthesized NO reduces cartilage proteoglycan synthesis in response to cytokines such as IL-1 [13]. IL-1 plays a pivotal role in the pathophysiology of OA by inducing a cascade of inflammatory and catabolic events, including the synthesis of prostaglandin E_2 (PGE_2) and NO. IL-1 also alters chondrocyte anabolism by suppressing the synthesis of extracellular matrix (ECM) components, such as proteoglycan and type II collagen, and by enhancing the production of matrix metalloproteinases (MMPs) [13].

Heterotopic ossification (HO) occurs when ectopic masses of endochondral and intramembranous bone form within the soft tissue and muscle around joints, in subcutaneous tissues, and in

ligaments [16]. HO that occurs around joints can result in pain, loss of motion, and impaired function. A number of recent studies have shown that there is an increased rate of HO in patients with serious injuries and head trauma [17]. A safe and effective primary prophylaxis for HO is under clinical investigation [18].

Grape seed proanthocyanidins (GSP) are powerful antioxidant polyphenols [19,20], and various epidemiologic and *in vivo*/*in vitro* experimental studies [21–23] have suggested that proanthocyanidins derived from fruits, vegetables, and beverages might decrease the risk of several lifestyle diseases. Recent studies have shown that proanthocyanidins have various therapeutic properties, such as radical scavenging, and exhibit a number of health benefits, including antiulcer, antiallergy, antidental caries, and antitumor activity. In addition, proanthocyanidins may inhibit food allergies, activate hair follicle growth, and protect cells from ultraviolet radiation [24–30].

Proanthocyanidins are obtained from many kinds of plants as a complex mixture of structurally related components. The structural diversity of polyphenols makes it difficult to determine the biological properties of individual components. The absorption of polyphenols also depends on their molecular weight. Because of their large molecular weight, proanthocyanidin polymers are likely not as easily absorbed by the small intestine. A major portion of ingested polyphenols (75–99%) is not detected in the urine, whereas procyanidin dimers are detected in the serum of rats and humans after GSP ingestion [31,32]. Procyanidin B3 (B3) is a procyanidin dimer that is widely studied due to its abundance in the human diet [33–35]. B3 and other procyanidin dimers can be absorbed by the small intestine [36] and have relevant antioxidant activities [37]. In the present study, we evaluated the role of B3 isolated from grape seed extracts in the differentiation and survival of chondrocytes *in vitro*. Furthermore, the potential ability of B3 to protect articular cartilage *in vivo* and prevent HO was estimated using a surgically-induced osteoarthritis model.

Materials and Methods

Reagents

B3 was isolated in the laboratory from proanthocyanidin-rich grape seed extracts, which contained 82% proanthocyanidins, provided by Kikkoman Co. (Chiba, Japan). Isolation was carried out according to the method by Zhao *et al.* [33]. Briefly, B3 was purified using reverse and normal phase HPLC. The isolated B3 was characterized by NMR and HPLC/MS, and the purity was determined to be 97% by HPLC/UV.

Animals

C57BL/6J mice were obtained from Sankyo Labo Service (Tokyo, Japan), and fed under standard conditions with food and water *ad libitum*. All of the animal experiments were approved by the Animal Care and Use Committee of Tokyo Medical and Dental University.

Cell Culture Conditions

The mouse chondrogenic ATDC5 cell line was obtained from the RIKEN cell bank (Tsukuba, Japan). Cells were maintained in DMEM/F12 (1:1) medium containing 5% FCS, 10 μg/ml human transferrin (Invitrogen A/S, Tastrup, Denmark), and 3×10^{-8} M sodium selenite (Sigma-Aldrich, Copenhagen, Denmark) at 37°C in a humidified atmosphere containing 5% CO_2. Chondrogenic differentiation of ATDC5 cells was performed as previously described [38]. Briefly, ATDC5 cells were seeded at a density of $6\times10^3\times$cells/cm^2 in 6-well or 24-well plates and cultured for 4 days. When cells became confluent, the medium was replaced with fresh medium supplemented with insulin (10 μg/ml).

Primary epiphyseal chondrocytes were isolated from 5-day-old mice as previously reported [39]. Briefly, cartilage tissues, including the femoral heads, femoral condyles and tibial plateau, were cut into small pieces and digested twice for 45 min each with 3 mg/ml type I collagenase. Then, the cartilage pieces were incubated in 0.5 mg/ml type I collagenase at 37°C in a thermal incubator with 5% CO_2 overnight. The next day, cell aggregates were dispersed via pipetting. The cells were cultured in 12-well plates with 5×10^4 cells per well in DMEM/F12 medium containing 10% FBS and antibiotics.

RNA Extraction and Real-time RT-PCR

Total RNA was extracted from chondrocytes and cell lines using TRIzol according to the manufacturer's directions. Real-time PCR was performed using the SuperScript III Platinum Two-Step qRT-PCR Kit with SYBR Green on the Mx3000P® QPCR System. Briefly, 0.5 μg total RNA was mixed with 10 μl 2× RT reaction mix and 2 μl RT, and then incubated for 30 min at 42°C. The reaction was terminated by heating for 5 min at 85°C. The cDNA mixture was then incubated for 30 min at 37°C in the presence of RNase H. The PCR reaction was carried out using a mixture of Platinum SYBR Green qRT-PCR Super-Mix UDG, the template cDNA, 10 mM of the primer mix, and DNase-free H_2O with a total volume of 20 μl per well. The cycling conditions were performed as indicated in the Invitrogen SuperScript™ III Platinum two-step qRT-PCR kit with SYBR Green. Gene expression was normalized to the endogenous control GAPDH, and fold changes in the genes of interest were determined using the comparative threshold cycle (Ct) method [40]. The qRT-PCR primers are listed in Table 1.

Measurement of Cellular Injury

Primary chondrocytes were incubated at 37°C in 96-well plates. After 2 days of culture, the medium was changed to 100 μl DMEM/F12 supplemented with 10% FBS. Subsequently, the cells were treated with H_2O_2, H_2O_2+B3 or Tween 20, as a positive control. After 24 h of culture, cellular injury was quantitated by measuring lactate dehydrogenase (LDH) release using an LDH Cytotoxicity Assay Kit (WAKO, Tokyo, Japan).

Surgical Induction of OA

Male mice (3 months old) were divided into two groups: B3 and control (n = 10 each). While the mice were under general anesthesia, a medial capsular incision was made and the left knee joint exposed. The medial collateral ligament was transected, and the medial meniscus was removed using a surgical microscope with a microsurgical technique, as previously reported [41]. The

Table 1. Primers for real-time PCR.

	Forward 5′-3′	Reverse 5′-3′
Gapdh	ACTCACGGCAAATTCAACGGC	ATCACAAACATGGGGGCATCG
Aggrecan	ATCAAGTGGAGCCGTGTTTC	CTGGGGATGTCGCATAAAAG
iNOS	GGATTTCAAAGACCTCTGGATC	ATACTTTATGCCACCAACAATGG
Col1a1	CACCCTCAAGAGCCTGAGTC	AGACGGCTGAGTAGGGAACA
Col2a1	CTGGCTGGCATCGTTAC	AGAGTGGTTCCCCTGGTGAG
Col10a1	ACCAGGAATGCCTTGTTCTC	ATGCTGAACGGGACCAAACG

doi:10.1371/journal.pone.0037728.t001

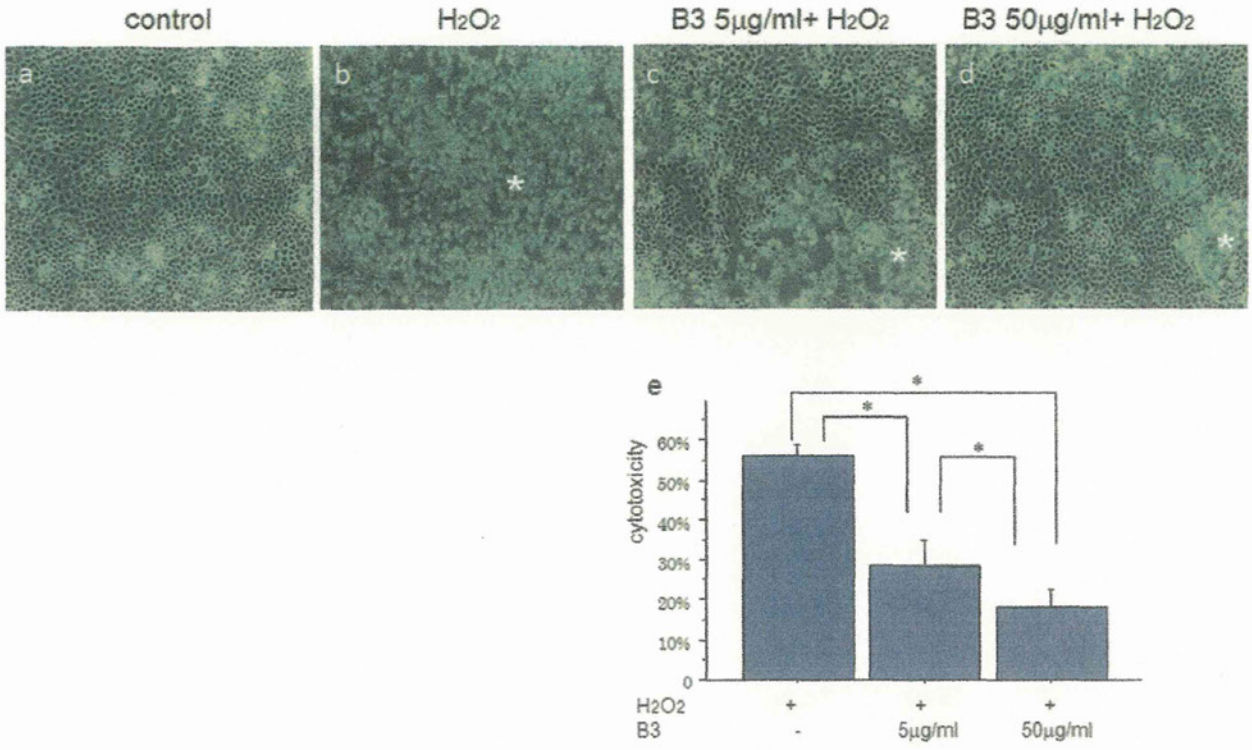

Figure 1. Phase contrast microscopy images of primary chondrocytes incubated with 500 μM H_2O_2 and increasing concentrations of B3 or vehicle control. The majority of H_2O_2 -treated cells were already detached and floating (b, asterisk), whereas control and B3-treated cells had started rounding but mostly remained adherent (c, d, asterisk). Scale bar = 200 μm. Cell viability of chondrocytes treated with H_2O_2 and B3 as determined by the LDH assay (e). B3 prevented H_2O_2-induced chondrocyte apoptosis in a dose-dependent manner. Values represent the mean and SD; n = 5 samples/group. *$p<0.05$.
doi:10.1371/journal.pone.0037728.g001

right knee underwent a sham operation. All of the animals were allowed unrestricted activity and were provided food and water *ad libitum*. None of the mice died during the experimental period. Five days after surgery, B3 or the vehicle control was administered orally (1 mg/10 g body weight) once a day.

Assessment of OA Severity

Whole knee joints were removed by dissection, fixed in 4% paraformaldehyde, and decalcified in EDTA. After dehydration and paraffin embedding, 5-μm frontal serial sections were cut from the whole knee joint. Two sections were obtained at 100-μm intervals and then stained with Safranin O–fast green and haematoxylin and eosin. The OA severity in the tibial plateau was evaluated according to Mankin's histologic grading system [42,43].

TUNEL Assay

The TUNEL assay was performed using a TUNEL detection kit according to the manufacturer's instructions (Takara Shuzo, Kyoto, Japan). Briefly, knee joint sections were incubated with 15 μg/ml of proteinase K for 15 min at room temperature and then washed with PBS. The sections were immersed in TdT Enzyme diluted with Labeling Safe Buffer (provided in the kit) and then incubated for 90 min at 37°C in a humid atmosphere. After washing in PBS, the slides were examined by fluorescence microscopy.

Immunohistochemistry

iNOS expression was examined by immunohistochemistry with anti-mouse iNOS antibody used according to the manufacturer's instructions (Abcam Biochemicals, Cambridge, UK). Briefly, tissue sections were incubated overnight at 4°C with a rabbit polyclonal anti-mouse iNOS antibody, followed by a 30-min incubation at room temperature with a biotinylated goat anti-rabbit IgG antibody. Next, the signal was visualized using peroxidase-conjugated avidin and diaminobenzidine from a Vectastain kit, according to the manufacturer's instructions (Vector Laboratories, Burlingame, CA, USA).

Statistical Analysis

Data are expressed as the mean ± SD. Statistical analysis was performed with the Mann–Whitney U test or Bonferroni/Dunn test. p values <0.05 were considered significant.

Results

Effects of B3 on H_2O_2-induced Chondrocyte Apoptosis

The protective effects of B3 against H_2O_2-mediated chondrocyte cell death were evaluated in epiphyseal primary chondrocytes. Cells were pre-incubated with increasing concentrations (5 and 50 μg/ml) of B3, and then treated with 500 μM H_2O_2. Treatment with H_2O_2 induced apoptosis in approximately 60% of the cells after 24 h of treatment. However, pre-incubating the cells with 5 and 50 μg/ml B3 significantly reduced the extent of apoptosis in a dose-dependent manner

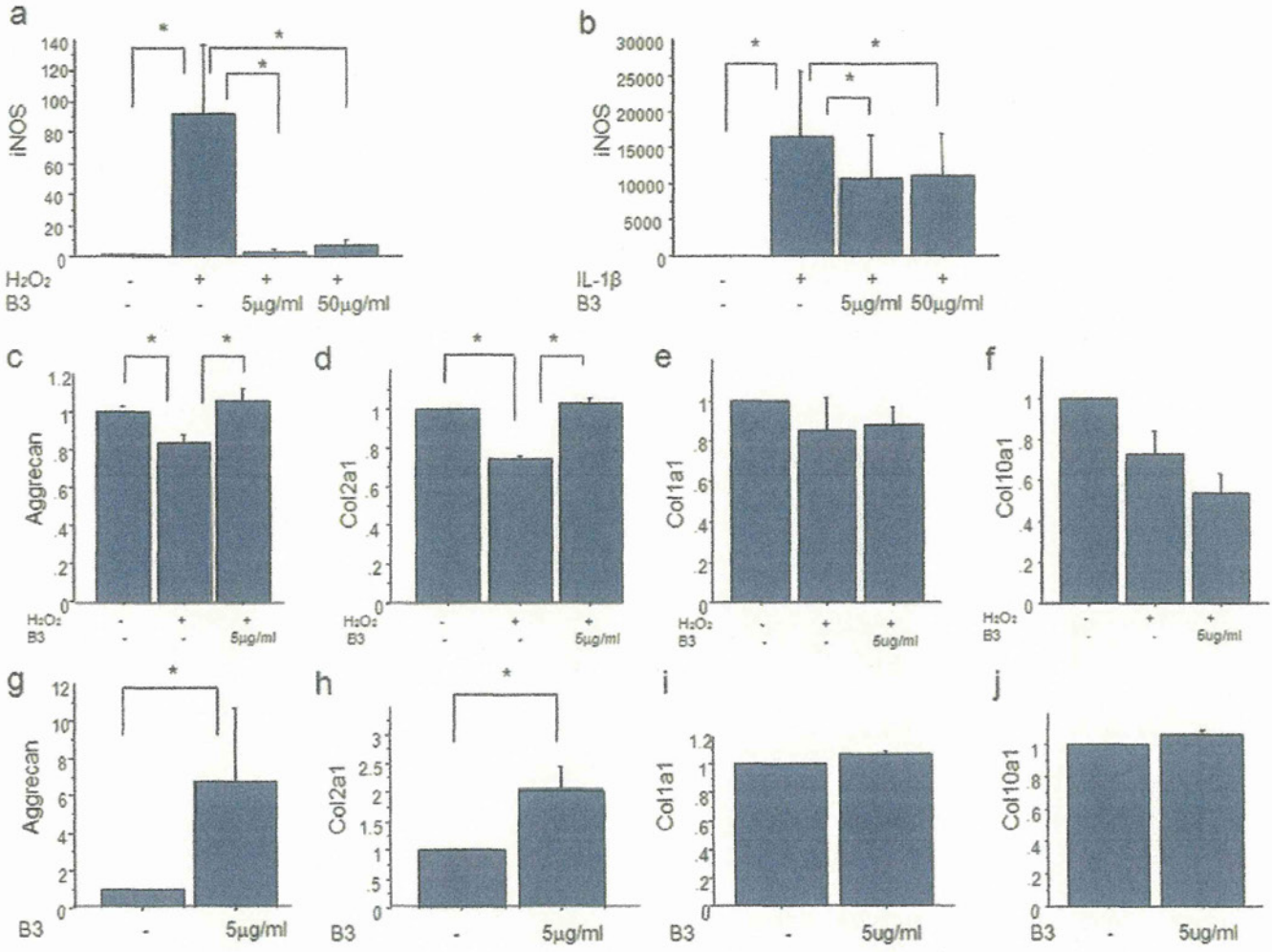

Figure 2. Effects of B3 on primary chondrocytes and ATDC5 cells. (a, b) B3 prevents H_2O_2- (a) or IL-1β(b)-induced iNOS synthesis. Primary chondrocytes were stimulated with 50 μM H_2O_2 in the absence or presence of increasing concentrations of B3 for 24 h. iNOS synthesis was assessed by real-time RT-PCR. Each column represents the mean ± SD of five separate experiments. *$p<0.05$. (c–f) B3 prevents H_2O_2-induced reduction of proteoglycan (c) and Col2a1 (d) synthesis. Primary chondrocytes were stimulated with 50 μM H_2O_2 in the absence or presence of 5 μg/ml B3 for 24 h. mRNA expression of proteoglycan (c), Col2a1 (d), Col1a1 (e) and Col10a1 (f) was assessed by real-time RT-PCR. Results represent the mean ± SEM of three independent experiments. *$p<0.05$ (g–j) B3 enhances aggrecan and Col2a1 synthesis in ATDC5 cells. ATDC5 cells were incubated in DMEM/F12 with 5%FBS. After the cells reached confluency, they were treated with differentiation medium. After 4 days of culture, the cells were treated with B3 or the vehicle control for 24 h. mRNA expression of aggrecan (g), Col2a1 (h), Col1a1 (i) and Col10a1 (j) were determined by real-timeRT-PCR. The results represent the mean ± SEM from three independent experiments. *$p<0.05$.
doi:10.1371/journal.pone.0037728.g002

(Figure 1). The concentrations of B3 were determined according to the results of a pilot study. Anti-apoptotic effects of B3 were observed from around 5 μg/ml to 1 μg/ml.

Effects of B3 on iNOS mRNA Expression in Chondrocytes

Primary chondrocytes were stimulated with 50 μM H_2O_2 in the absence or presence of increasing concentrations of B3, and iNOS production was evaluated by real-time RT-PCR. B3 treatment suppressed H_2O_2-induced iNOS production (Figure 2a). Similarly, iNOS production stimulated by 10 ng/ml IL-1β was also suppressed in the presence of B3 (Figure 2b). An LDH assay demonstrated that this inhibition was not due to reduced cell viability (data not shown).

Effects of B3 on Chondrocyte ECM Synthesis

To investigate the effects of B3 on H_2O_2-induced reduction of chondrocyte differentiation marker gene expression, primary chondrocytes were stimulated with H_2O_2 in the absence or presence of increasing concentrations of B3 for 24 h. B3 treatment inhibited the H_2O_2-induced decrease in mRNA expression of chondrocyte differentiation markers, including aggrecan and Col2a1 (Figure 2c and d). By contrast, the expression of the chondrocyte hypertrophy markers Col1a1 and Col10a1 was not affected by B3 treatment (Figure 2e and f).

Next, we evaluated the effects of B3 on chondrocyte differentiation using ATDC5 cells. ATDC5 cells were grown to confluency and then cultured in differentiation medium. After 4 days, the cells were treated with B3 for 24 h. mRNA synthesis of aggrecan and Col2a1, was significantly enhanced by B3

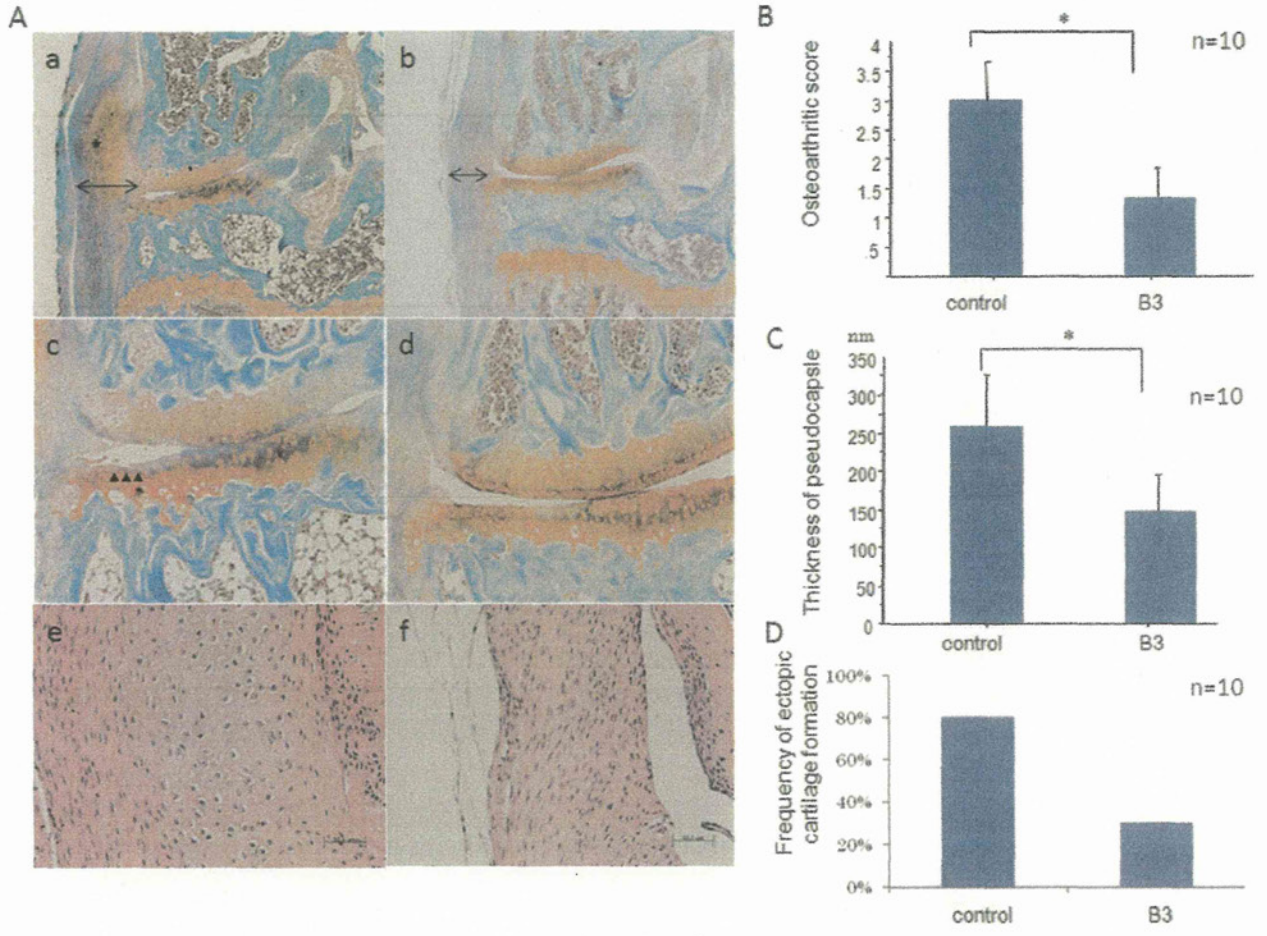

Figure 3. Histological analysis of surgically-induced osteoarthritis (OA) in the knee joints of mice after administering B3 or the vehicle control. OA was surgically induced in 12-week-old mice, and the knee joints were harvested 4 weeks later. B3 or the vehicle alone (control) was orally administered 5 times a week beginning 5 days after surgery and continuing until the end of the experiment (n = 10). A, Representative histologic features (a–d, Safranin O staining; e and f, H&E staining) of the knee joints of control (a, c, e) and B3-treated (b, d, f) mice. Degenerative changes in the articular cartilage were ameliorated in B3-treated mice (b, d) as compared to controls (a, c). Note the thicker medial pseudocapsule in the control group (a, b, arrows), and the ectopic cartilage formation in the pseudocapsule (a, asterisk). e, f, High magnification images of the pseudocapsules. Note that the control pseudocapsule is occupied with hypertrophic chondrocyte-like cells (e), whereas only thin fibrous cells are observed in B3-treated mice (f). B, Histological scoring of cartilage destruction according to Mankin's score, * $p<0.05$. C, The thickness of the pseudocapsule was significantly reduced in the B3-treated group. Values represent the mean ± SD of 10 samples per group. *$p<0.05$. D, The incidence of ectopic cartilage formation at the medial pseudocapsule was reduced by B3 treatment.
doi:10.1371/journal.pone.0037728.g003

treatment (Figure 2g and h), while Col1a1 and Col10a1 expression was not affected (Figure 2i and j).

Prevention of Cartilage Destruction and Ectopic Cartilage Formation by B3 Administration in a Surgically-induced OA Model

To examine whether B3 prevents cartilage destruction, OA was surgically induced in C57BL/6J mice, then B3 or a vehicle control was orally administered. OA was induced by performing a medial collateral ligament transection and medial meniscectomy on the left knees; sham operations were performed on the right knees. B3 or the vehicle control was administered orally 5 days/week beginning 5 days after the operation, and mice were euthanized 4 weeks after the operation. Histological examination revealed that B3 administration markedly protected the articular cartilage from proteoglycan depletion and prevented alterations in surface structure (Figure 3Aa–d). The Mankin's histologic OA grading score in B3-treated animals was ~50% of the values in the control group ($p<0.05$, Figure 3B).

In this OA model, the medial meniscus and medial collateral ligament are surgically removed, followed by formation of a pseudocapsule, which is composed of fibrous tissues. In control OA mice, ectopic cartilaginous tissues were frequently observed in the thick pseudocapsule as a result of chronic inflammation (Figure 3Aa and e). By contrast, the thickness of the pseudocapsule was markedly reduced in B3-treated mice along with a reduced frequency of ectopic cartilage formation (Figure 3Ab and f, C and D). These observations suggested that B3 suppressed chronic inflammation in the surgical region.

Chondrocyte apoptosis is increased in OA cartilage [2,44]. These observations prompted us to investigate the effects of B3 administration on chondrocyte apoptosis. TUNEL-positive cells were abundant among chondrocytes in the superficial layer of articular cartilage in control mice with surgically-induced OA,

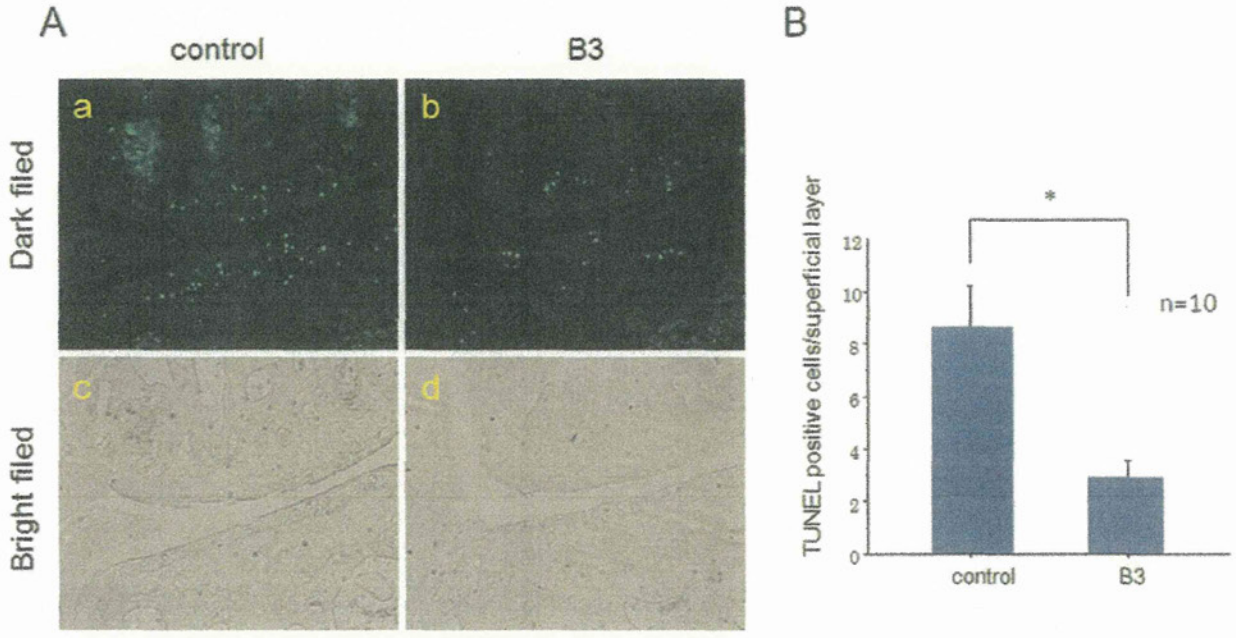

Figure 4. A. TUNEL staining of OA cartilage sections. TUNEL staining was examined by dark-field (a and b) and bright-field (c and d) microscopy. The number of TUNEL-positive cells was increased in the superficial layer of joint cartilage in OA control mice (a), but was significantly reduced in B3-treated mice (b). B, The number of TUNEL-positive cells in the superficial layer of articular cartilage as determined by fluorescence microscopy. Values represent the mean ± SD of 10 mice per group. *$p<0.05$ (Mann−Whitney U test).
doi:10.1371/journal.pone.0037728.g004

whereas TUNEL-positive cells were rarely observed in B3-treated mice (Figure 4Aa and b). The number of TUNEL-positive chondrocytes at the superficial layer of the joint cartilage in the B3-treated group was almost one-third of that observed in the control group ($p<0.05$, Figure 4B). These data indicated that the antiapoptotic effects of B3 protected the articular cartilage.

To examine if B3 supplementation prevented cartilage destruction by inhibiting iNOS expression, immunohistological analysis for iNOS was performed. iNOS protein expression was enhanced in the synovial tissues and the pseudocapsule around the surgical region in control mice (Figure 5a, arrows), whereas its expression was reduced by B3 administration (Figure 5b). These data indicated that B3 prevented aberrant articular cartilage degeneration and heterotopic cartilage formation, at least in a part, through suppression of iNOS in the OA model.

Discussion

Chondrocyte apoptosis has been implicated in the pathogenesis of degenerative joint diseases, including osteoarthritis and rheumatoid arthritis [1,2,10]. H_2O_2 is both exogenously supplied and endogenously produced in rheumatoid arthritis [1], and it can induce chondrocyte apoptosis [10]. Thus, we used H_2O_2-treated chondrocytes as an *in vitro* model to examine the ability of B3 to prevent chondrocyte apoptosis. Indeed, B3 blocked H_2O_2-induced chondrocyte apoptosis *in vitro*.

In this study, both H_2O_2 and the inflammatory cytokine IL-1ß induced iNOS mRNA expression in chondrocytes, and B3 significantly suppressed iNOS mRNA expression arising from both stimuli (Figure 2). The iNOS and NO levels in the synovial uid and serum of patients with osteoarthritis are higher than those in healthy individuals [45,46]. iNOS is expressed following stimulation with a variety of inflammatory agents, such as endotoxins or cytokines [47], and leads to the production of NO in inammatory settings.

NO induces oxidative stress in chondrocytes, and as a result, enhances aggrecan degradation and chondrocyte apoptosis [3,11]. NO also attenuates the synthesis of cartilage matrix proteins [48–50]. In our study, H_2O_2 reduced mRNA synthesis of aggrecan and Col2a1, which are cartilage differentiation markers, while B3 significantly prevented these negative effects.

In this study, B3 administration markedly prevented OA progression in articular cartilage. Reduced progression of experimental osteoarthritis is observed *in vivo* upon the selective inhibition of iNOS [51]. Furthermore, selective inhibition of iNOS reduces the progression of experimental osteoarthritis *in vivo* [52]. In a collagen-induced arthritis model, joint pathology is significantly inhibited in NOS-deficient mice [13]. These findings are consistent with our observation that orally administered B3 prevents chondrocyte degeneration via regulating iNOS synthesis, as shown in our surgically-induced OA model. Although B3-mediated iNOS inhibition may be one means by which B3 prevents OA, the molecular target of B3 is still unknown.

Furthermore, TUNEL staining revealed that B3 suppressed chondrocyte apoptosis in a mouse OA model. Many studies have shown that apoptotic cell death occurs at an increased rate in osteoarthritic cartilage, detrimentally impacting articular cartilage maintenance. Combined with the *in vitro* data, this observation may indicate that B3 had both antioxidant and anti-inflammatory effects.

We also demonstrated that B3 treatment prevented heterotopic cartilage formation near the surgical region, but enhanced the differentiation of chondrocyte-like ATDC5 cells *in vitro*. This discrepancy may be due to the effects of B3 on abnormal inflammation at the pseudocapsule. In this study, ectopic cartilage formation was triggered by the trauma of knee surgery, *e.g.*,

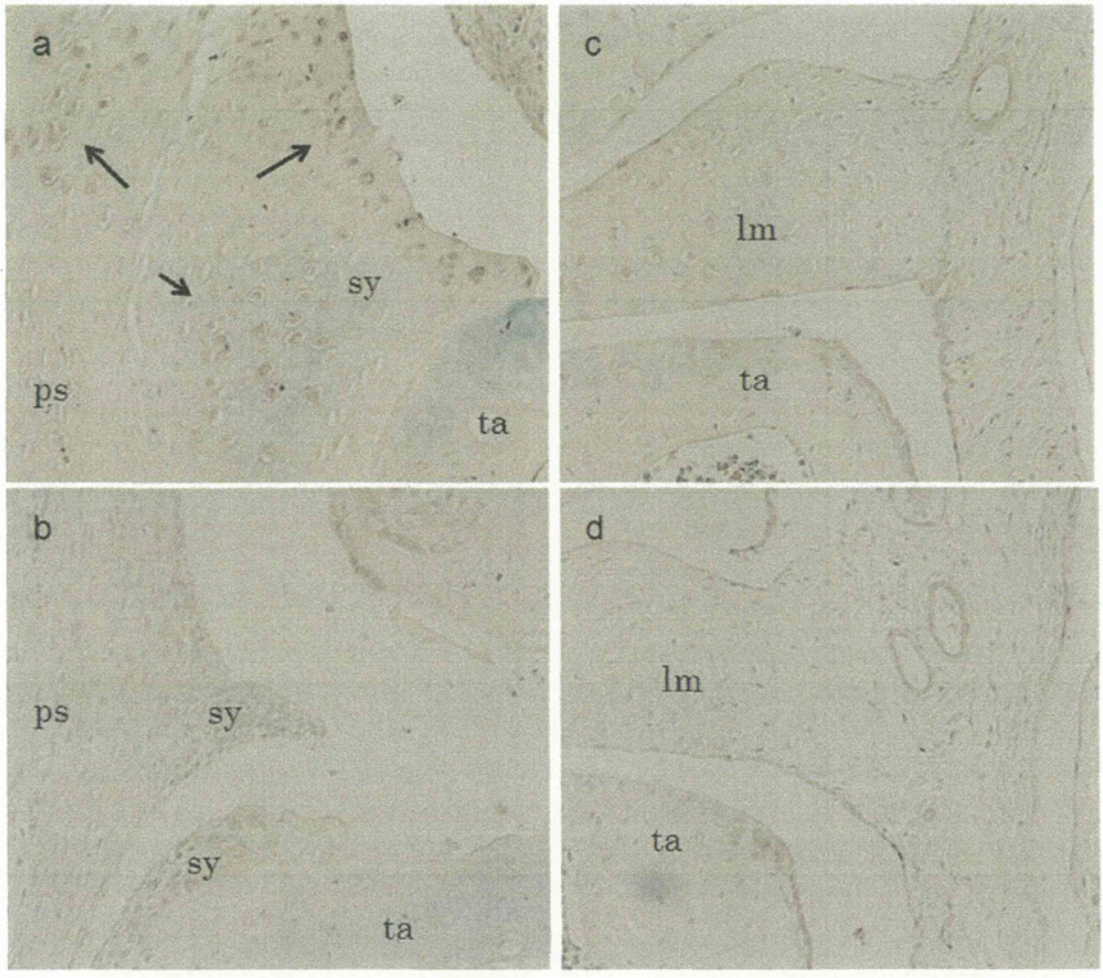

Figure 5. iNOS expression in a murine OA model. iNOS protein expression was enhanced in the synovial tissues and the pseudocapsule around the surgical region in control mice (a, arrows), but was reduced in animals receiving B3 (b). iNOS expression and background levels were similar at the lateral region of each knee joint in B3-treated (d) and control mice (c). sy, synovium; ps, pseudocapsule; lm, lateral meniscus; ta, tibial articular cartilage.
doi:10.1371/journal.pone.0037728.g005

resection of the meniscus and medial collateral ligament, and a fibrous pseudocapsule was formed. In this location, a cascade of chronic inflammation likely occurred as a result of joint instability. In a typical cascade, iNOS is first expressed following stimulation with a variety of inflammatory agents, such as endotoxins or cytokines [47]. Then, NO promotes inflammation by enhancing the production of inflammatory cytokines [53] and prostaglandins [54]. The latter are implicated in the formation of heterotopic bone [55]. On a related note, anthocyanins inhibit NF-κB activation via TNF-α, resulting in the inhibition of VEGF expression [56]. The NF-κB pathway is involved in regulating prostaglandin expression via COX-2 activation [57,58]. Thus, B3 may prevent heterotopic ossification by inhibiting prostaglandin activity through suppression of iNOS synthesis and inactivation of the NF-κB pathway.

GSP have several bioactivities. They limit adipogenesis and function as insulinomimetic, anti-inflammatory, and antioxidant agents as shown in this study [32]. Dimeric and trimeric oligomers are the most powerful procyanidin molecules that most closely mimic complete GSP [32]. Grape seed extracts might be expected to have same efficiency because they include several procyanidin dimers and trimers in addition to B3, but additional experiments will be required to confirm this hypothesis.

In conclusion, we have demonstrated that B3 prevented cartilage destruction in an experimental murine model of OA and heterotopic cartilage formation. Our results suggest that B3 prevented chondrocyte apoptosis by directly affecting chondrocytes *in vivo*. These results support the potential therapeutic applications of B3 in humans with OA and HO.

Author Contributions

Conceived and designed the experiments: YA. Performed the experiments: HA HO MI DK. Analyzed the data: YA HA. Contributed reagents/materials/analysis tools: MO AS AO. Wrote the paper: YA.

References

1. Kim HA, Song YW (1999) Apoptotic chondrocyte death in rheumatoid arthritis. Arthritis Rheum 42: 1528–1537.
2. Kim HA, Lee YJ, Seong SC, Choe KW, Song YW (2000) Apoptotic chondrocyte death in human osteoarthritis. J Rheumatol 27: 455–462.
3. Kuhn K, D'Lima DD, Hashimoto S, Lotz M (2004) Cell death in cartilage. Osteoarthritis Cartilage. England. pp 1–16.
4. Cheng AW, Stabler TV, Bolognesi M, Kraus VB (2011) Selenomethionine inhibits IL-1beta inducible nitric oxide synthase (iNOS) and cyclooxygenase 2 (COX2) expression in primary human chondrocytes. Osteoarthritis Cartilage. England: 2010 Osteoarthritis Research Society International. Published by Elsevier Ltd.. pp 118–125.
5. Diaz-Gallego L, Prieto JG, Coronel P, Gamazo LE, Gimeno M, et al. (2005) Apoptosis and nitric oxide in an experimental model of osteoarthritis in rabbit after hyaluronic acid treatment. J Orthop Res. United States. pp 1370–1376.
6. Fukuda K, Kumano F, Takayama M, Saito M, Otani K, et al. (1995) Zonal differences in nitric oxide synthesis by bovine chondrocytes exposed to interleukin-1. Inflamm Res 44: 434–437.
7. Blanco FJ, Guitian R, Vázquez-Martul E, de Toro FJ, Galdo F (1998) Osteoarthritis chondrocytes die by apoptosis: A possible pathway for osteoarthritis pathology. Arthritis & Rheumatism 41: 284–289.
8. Kühn K, Shikhman AR, Lotz M (2003) Role of nitric oxide, reactive oxygen species, and p38 MAP kinase in the regulation of human chondrocyte apoptosis. Journal of Cellular Physiology 197: 379–387.
9. Shah R, Raska K, Tiku MI. (2005) The presence of molecular markers of in vivo lipid peroxidation in osteoarthritic cartilage: a pathogenic role in osteoarthritis. Arthritis Rheum 52: 2799–2807.
10. Asada S, Fukuda K, Nishisaka F, Matsukawa M, Hamanisi C (2001) Hydrogen peroxide induces apoptosis of chondrocytes; involvement of calcium ion and extracellular signal-regulated protein kinase. Inflamm Res 50: 19–23.
11. Clancy RM, Abramson SB, Kolme C, Rediske J (1997) Nitric oxide attenuates cellular hexose monophosphate shunt response to oxidants in articular chondrocytes and acts to promote oxidant injury. J Cell Physiol. United States. pp 183–191.
12. Beck KF, Eberhardt W, Walpen S, Apel M, Pfeilschifter J (1998) Potentiation of nitric oxide synthase expression by superoxide in interleukin 1 beta-stimulated rat mesangial cells. FEBS Lett. Netherlands. pp 35–38.
13. Taskiran D, Stefanovicracic M, Georgescu H, Evans C (1994) Nitric-Oxide Mediates Suppression of Cartilage Proteoglycan Synthesis by Interleukin-1. Biochemical and Biophysical Research Communications 200: 142–148.
14. Kim J, Xu M, Xo R, Mates A, Wilson G, et al. (2010) Mitochondrial DNA damage is involved in apoptosis caused by pro-inflammatory cytokines in human OA chondrocytes. Osteoarthritis Cartilage 18: 424–432.
15. Stevens AL, Wheeler CA, Tannenbaum SR, Grodzinsky AJ (2008) Nitric oxide enhances aggrecan degradation by aggrecanase in response to TNF-alpha but not IL-1beta treatment at a post-transcriptional level in bovine cartilage explants. Osteoarthritis Cartilage. England. pp 489–497.
16. Brooker AF, Bowerman JW, Robinson RA, Riley LH Jr. (1973) Ectopic ossification following total hip replacement. Incidence and a method of classification. J Bone Joint Surg Am 55: 1629–1632.
17. Hosalkar H, Pandya NK, Hsu J, Keenan MA (2011) What's new in orthopaedic rehabilitation. J Bone Joint Surg Am 93: 1367–1374.
18. Hamid N, Ashraf N, Bosse MJ, Connor PM, Kellam JF, et al. (2010) Radiation therapy for heterotopic ossification prophylaxis acutely after elbow trauma: a prospective randomized study. J Bone Joint Surg Am. United States. pp 2032–2038.
19. Yamaguchi F, Yoshimura Y, Nakazawa H, Ariga T (1999) Free radical scavenging activity of grape seed extract and antioxidants by electron spin resonance spectrometry in an H(2)O(2)/NaOH/DMSO system. J Agric Food Chem. United States. pp 2544–2548.
20. Koga T, Moro K, Nakamori K, Yamakoshi J, Hosoyama H, et al. (1999) Increase of antioxidative potential of rat plasma by oral administration of proanthocyanidin-rich extract from grape seeds. J Agric Food Chem. United States. pp 1892–1897.
21. Yamakoshi J, Sano A, Tokutake S, Saito M, Kikuchi M, et al. (2004) Oral intake of proanthocyanidin-rich extract from grape seeds improves chloasma. Phytother Res 18: 895–899.
22. Yamakoshi J, Otsuka F, Sano A, Tokutake S, Saito M, et al. (2003) Lightening effect on ultraviolet-induced pigmentation of guinea pig skin by oral administration of a proanthocyanidin-rich extract from grape seeds. Pigment Cell Res. Denmark. pp 629–638.
23. Yamakoshi J, Saito M, Kataoka S, Tokutake S (2002) Procyanidin-rich extract from grape seeds prevents cataract formation in hereditary cataractous (ICR/f) rats. J Agric Food Chem. United States. pp 4983–4988.
24. Akiyama H, Sakushima J, Taniuchi S, Kanda T, Yanagida A, et al. (2000) Antiallergic effect of apple polyphenols on the allergic model mouse. Biol Pharm Bull 23: 1370–1373.
25. Akiyama H, Sato Y, Watanabe T, Nagaoka MH, Yoshioka Y, et al. (2005) Dietary unripe apple polyphenol inhibits the development of food allergies in murine models. FEBS Lett. Netherlands. pp 4485–4491.
26. Carini M, Aldini G, Bombardelli E, Morazzoni P, Maffei Facino R (2000) UVB-induced hemolysis of rat erythrocytes: protective effect of procyanidins from grape seeds. Life Sci. England. pp 1799–1814.
27. Hibasami H, Shohji T, Shibuya I, Higo K, Kanda T (2004) Induction of apoptosis by three types of procyanidin isolated from apple (Rosaceae Malus pumila) in human stomach cancer KATO III cells. Int J Mol Med 13: 795–799.
28. Takahashi T, Kamiya T, Hasegawa A, Yokoo Y (1999) Procyanidin oligomers selectively and intensively promote proliferation of mouse hair epithelial cells in vitro and activate hair follicle growth in vivo. J Invest Dermatol 112: 310–316.
29. Yanagida A, Kanda T, Tanabe M, Matsudaira F, Oliveira Cordeiro JG (2000) Inhibitory effects of apple polyphenols and related compounds on cariogenic factors of mutans streptococci. J Agric Food Chem. United States. pp 5666–5671.
30. Ariga T (2004) The antioxidative function, preventive action on disease and utilization of proanthocyanidins. Biofactors 21: 197–201.
31. Sano A, Yamakoshi J, Tokutake S, Tobe K, Kubota Y, et al. (2003) Procyanidin B1 is detected in human serum after intake of proanthocyanidin-rich grape seed extract. Biosci Biotechnol Biochem 67: 1140–1143.
32. Serra A, Macia A, Romero MP, Valls J, Blade C, et al. (2010) Bioavailability of procyanidin dimers and trimers and matrix food effects in in vitro and in vivo models. Br J Nutr. England. pp 944–952.
33. Zhao J, Wang J, Chen Y, Agarwal R (1999) Anti-tumor-promoting activity of a polyphenolic fraction isolated from grape seeds in the mouse skin two-stage initiation-promotion protocol and identification of procyanidin B3–3'-gallate as the most effective antioxidant constituent. Carcinogenesis 20: 1737–1745.
34. Carando S, Teissedre PL, Pascual-Martinez L, Cabanis JC (1999) Levels of flavan-3-ols in French wines. J Agric Food Chem. United States. pp 4161–4166.
35. Quinde-Axtell Z, Baik BK (2006) Phenolic compounds of barley grain and their implication in food product discoloration. J Agric Food Chem 54: 9978–9984.
36. Deprez S, Mila I, Huneau JF, Tome D, Scalbert A (2001) Transport of proanthocyanidin dimer, trimer, and polymer across monolayers of human intestinal epithelial Caco-2 cells. Antioxid Redox Signal 3: 957–967.
37. Oizumi Y, Mohri Y, Hirota M, Makabe H (2010) Synthesis of procyanidin B3 and its anti-inflammatory activity. the effect of 4-alkoxy group of catechin electrophile in the Yb(OTf)(3)-catalyzed condensation with catechin nucleophile. J Org Chem 75: 4884–4886.
38. Shukunami C, Shigeno C, Atsumi T, Ishizeki K, Suzuki F, et al. (1996) Chondrogenic differentiation of clonal mouse embryonic cell line ATDC5 in vitro: differentiation-dependent gene expression of parathyroid hormone (PTH)/PTH-related peptide receptor. The Journal of Cell Biology 133: 457–468.
39. Gosset M, Berenbaum F, Thirion S, Jacques C (2008) Primary culture and phenotyping of murine chondrocytes. Nat Protocols 3: 1253–1260.
40. Pfaffl MW (2001) A new mathematical model for relative quantification in real-time RT-PCR. Nucleic Acids Res 29: e45.
41. Kamekura S, Kawasaki Y, Hoshi K, Shimoaka T, Chikuda H, et al. (2006) Contribution of runt-related transcription factor 2 to the pathogenesis of osteoarthritis in mice after induction of knee joint instability. Arthritis & Rheumatism 54: 2462–2470.
42. Mankin HJ, Dorfman H, Lippiello L, Zarins A (1971) Biochemical and metabolic abnormalities in articular cartilage from osteo-arthritic human hips. II. Correlation of morphology with biochemical and metabolic data. J Bone Joint Surg Am 53: 523–537.
43. Mankin HJ (1973) Biochemical and metabolic abnormalities in osteoarthritic human cartilage. Fed Proc 32: 1478–1480.
44. Hashimoto S, Ochs RL, Komiya S, Lotz M (1998) Linkage of chondrocyte apoptosis and cartilage degradation in human osteoarthritis. Arthritis Rheum 41: 1632–1638.
45. Yoo HS, Lee EA, Yoon JJ, Park TG (2005) Hyaluronic acid modified biodegradable scaffolds for cartilage tissue engineering. Biomaterials. England. pp 1925–1933.
46. Hakansson L, Hallgren R, Venge P (1980) Regulation of granulocyte function by hyaluronic acid. In vitro and in vivo effects on phagocytosis, locomotion, and metabolism. J Clin Invest 66: 298–305.
47. Scher JU, Pillinger MH, Abramson SB (2007) Nitric oxide synthases and osteoarthritis. Curr Rheumatol Rep 9: 9–15.
48. Manciro E, Lopez-Armada MJ, de Andres MC, Carames B, Martin MA, et al. (2005) Effect of nitric oxide on mitochondrial respiratory activity of human articular chondrocytes. Ann Rheum Dis. England. pp 388–395.
49. Andreutti D, Geinoz A, Gabbiani G (1999) Effect of hyaluronic acid on migration, proliferation and alpha-smooth muscle actin expression by cultured rat and human fibroblasts. J Submicrosc Cytol Pathol 31: 173–177.
50. Lotz M (1999) The role of nitric oxide in articular cartilage damage. Rheum Dis Clin North Am 25: 269–282.
51. Pelletier JP, Jovanovic D, Fernandes JC, Manning P, Connor JR, et al. (1998) Reduced progression of experimental osteoarthritis in vivo by selective inhibition of inducible nitric oxide synthase. Arthritis Rheum 41: 1275–1286.
52. Pelletier JP, Jovanovic DV, Lascau-Coman V, Fernandes JC, Manning PT, et al. (2000) Selective inhibition of inducible nitric oxide synthase reduces progression of experimental osteoarthritis in vivo: possible link with the reduction in chondrocyte apoptosis and caspase 3 level. Arthritis Rheum 43: 1290–1299.

53. McInnes IB, Leung BP, Field M, Wei XQ, Huang FP, et al. (1996) Production of nitric oxide in the synovial membrane of rheumatoid and osteoarthritis patients. J Exp Med 184: 1519–1524.
54. Salvemini D, Misko TP, Masferrer JL, Seibert K, Currie MG, et al. (1993) Nitric oxide activates cyclooxygenase enzymes. Proc Natl Acad Sci U S A 90: 7240–7244.
55. Bartlett CS, Rapuano BE, Lorich DG, Wu T, Anderson RC, et al. (2006) Early changes in prostaglandins precede bone formation in a rabbit model of heterotopic ossification. Bone. United States. pp 322–332.
56. Nizamutdinova IT, Kim YM, Chung JI, Shin SC, Jeong YK, et al. (2009) Anthocyanins from black soybean seed coats stimulate wound healing in fibroblasts and keratinocytes and prevent inflammation in endothelial cells. Food Chem Toxicol. England. pp 2806–2812.
57. Crofford LJ, Tan B, McCarthy CJ, Hla T (1997) Involvement of nuclear factor kappa B in the regulation of cyclooxygenase-2 expression by interleukin-1 in rheumatoid synoviocytes. Arthritis Rheum 40: 226–236.
58. Eisengart CA, Mestre JR, Naama HA, Mackrell PJ, Rivadeneira DE, et al. (2000) Prostaglandins regulate melanoma-induced cytokine production in macrophages. Cell Immunol. United States: 2000 Academic Press. pp 143–149.

Japanese Journal of Applied Physics **51** (2012) 07GF15 **REGULAR PAPER**
DOI: 10.1143/JJAP.51.07GF15

Elasticity Evaluation of Regenerating Cartilage Sample Based on Laser Doppler Measurement of Ultrasonic Particle Velocity

Naotaka Nitta*, Masaki Misawa, Kazuhiro Homma, and Tsuyoshi Shiina[1]

Human Technology Research Institute, National Institute of Advanced Industrial Science and Technology (AIST), Tsukuba, Ibaraki 305-8564, Japan
[1]*Human Health Science, Graduate School of Medicine, Kyoto University, Kyoto 606-8507, Japan*

Received November 19, 2011; accepted April 16, 2012; published online July 20, 2012

It is important for regenerative medicine to evaluate the maturity of regenerating tissue. In the maturity evaluation of regenerating cartilage, it is useful to measure the temporal change of elasticity because the maturity of regenerating tissue is closely related to its elasticity. In this study, an elasticity evaluation method for the extracted regenerating cartilage sample, which is based on the laser Doppler measurement of ultrasonic particle velocity, was experimentally investigated using agar-based phantoms with different elastic moduli and the regenerating cartilage samples extracted from beagles in animal experiments. In addition, the experimentally-obtained elasticity was compared with the result of a static compression test. These results verified the feasibility of the proposed method in the elasticity evaluation of regenerating cartilage samples.

1. Introduction

Diagnosis for hard tissue is becoming increasingly important with the increase of aging population. Therefore, quantitative evaluation and analysis methods for bone are actively studied.[1–6] Similarly, quantitative evaluation for cartilage is also important. For example, osteoarthritis (OA) is one of the most common disorders found in the aging population. In the degenerative cartilage, the tension of the superficial layer of collagen fiber decreases gradually.[7–10] One of the most important properties in the cartilage is the mechanical property or elasticity. With the aim of diagnosing and evaluating such properties, some evaluation methods using magnetic resonance (MR) imaging are studied.[11–13]

For *in vitro* evaluation of cartilage using ultrasound, acoustic microscopy,[14–17] sound speed measurement,[18–21] attenuation measurement,[22] reflected wave or backscatter analysis,[23–28] and an elastographic (compressive) approach based on the echo shift measurement due to the cartilage compression[29,30] have been studied. For *in vivo* evaluation of cartilage, reflected wave analysis, evaluation of roughness of the cartilage surface, thickness measurement, and power Doppler evaluation using an ultrasound diagnosis device have been studied.[31–35] Moreover, as a less-invasive approach, reflected wave analysis using intravascular ultrasound has also been studied.[36] Among these methods, the more direct approach for elasticity evaluation is the mechanical compression-based method. Although the sound speed is a promising parameter for elasticity evaluation, it is affected by the density of cartilage.

On the other hand, as a solution to recover such degenerated or deficient cartilage, regenerative medicine has been addressed. In typical regenerative medicine for cartilage recovery, a cell-seeded scaffold is cultured over a period of time and then the cultured scaffold is transplanted into the body. Here, the evaluation of the cultured scaffold before and after transplantation is essential for ensuring its adequate maturity before and after transplantation. In the maturity evaluation of regenerating cartilage, it is useful to measure the temporal change of elasticity because the maturity of regenerating tissue is closely related to its elasticity.[37] As the maturity evaluation, sound speed and attenuation measurements by acoustic microscopy have been reported.[38] However, since the sound speed is affected by the density and elastic moduli, the direct elasticity evaluation based on the sound speed is difficult. Moreover, since the cultured scaffold before transplantation is the sole material, nondestructive measurements are required for elasticity evaluation.

In this study, with the evaluation of cultured scaffold samples before transplantation in mind, we propose an elasticity evaluation method for extracted regenerating cartilage samples. In the proposed method, with the aim of realizing nondestructive and compression-based evaluation of elasticity, the ultrasound itself is newly used instead of an indenter. Moreover, a laser Doppler measurement is conducted for the ultrasonic particle velocity as the response to the ultrasound irradiation. The feasibility of this method is experimentally investigated using agar-based phantoms with different elastic moduli and regenerating cartilage samples extracted from beagles in animal experiments.

2. Methods

For example, articular cartilage is composed of water, an extracellular matrix including collagen and proteoglycan, and chondrocyte. In general, the water content of cartilage tissue is high and about 80% by weight percent ratio. On the basis of such compositions, the biphasic theory has been proposed[39] and is widely accepted as a mechanical model of cartilage tissue. In this theory, it is assumed that the cartilage tissue is a composite body with an incompressible liquid phase and a solid phase. Considering that the cartilage tissue contains lots of incompressible liquid or water, the assumption that the entire cartilage tissue has a slightly compressible property is reasonable. In this study, with the aim of simplifying the problem of elasticity evaluation for cartilage tissue with the above-mentioned property, the cartilage tissue is assumed to be a nearly incompressible, isotropic, and linear elastic body. In other words, it is assumed that the influence of the shear modulus is sufficiently small and negligible although it is not zero.

Figure 1 shows the principle of the proposed method. Here, ultrasound is irradiated from the bottom of the sample and the particle velocity on the sample surface is measured.

*E-mail address: n.nitta@aist.go.jp

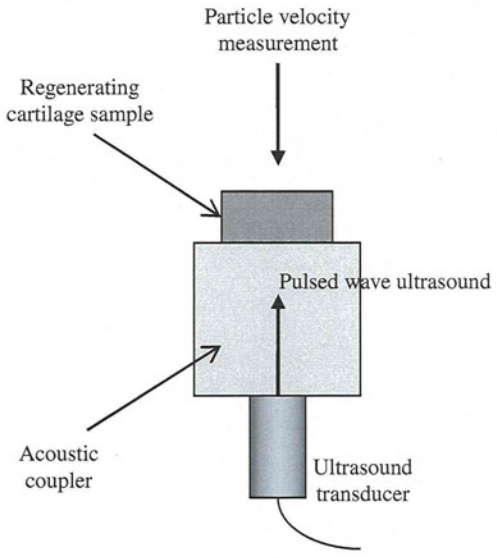

Fig. 1. Principle of the proposed method.

Since the particle velocity is continuous at the boundary between media with different acoustic impedances, the particle velocity on the surface boundary of a sample is equivalent to that inside the sample. On the basis of the above assumptions and another assumption that the entire cartilage tissue sample is homogeneous, when only the plane progressive wave of a longitudinal wave propagates in the homogeneous cartilage sample, the particle velocity v_i is expressed as

$$v_i = \sqrt{2} v_i' e^{j\omega_0 t}, \tag{1}$$

where v_i', ω_0, and t indicate the effective value of particle velocity, angular frequency, and time, respectively. The index i of v_i' means the incident wave, that is, the progressive wave in the sample. The effective value of particle velocity v_i' is expressed as follows, by using the effective value of velocity potential ϕ_i' ($= |\phi_i'| e^{-jkx}$):

$$v_i' = jk\phi_i', \tag{2}$$

where k ($= \omega_0/c$) is the wavelength constant, x indicates the propagation direction of the plane wave, and c is the sound speed of the longitudinal wave in the sample.

Next, the particle displacement u_i is derived as follows, by integrating the particle velocity v_i with respect to time:

$$u_i = \sqrt{2} u_i' e^{j\omega_0 t}, \tag{3}$$

where u_i' is the effective value of particle displacement and is expressed as follows:

$$u_i' = \frac{1}{c}\phi_i', \tag{4}$$

where u_i' is a function of x. To attain elasticity information, strain ε_i' is derived as follows, by differentiating u_i' with respect to x:

$$\varepsilon_i' = -j\frac{k}{c}\phi_i'. \tag{5}$$

The above particle displacement and strain are induced by local stress along the propagation direction of a plane wave in the acoustic field. Assuming that the stress in the inside and boundary of the sample is induced by an incident wave in the sample, the stress σ_i' is expressed as follows:

$$\sigma_i' = j\omega_0 \rho \phi_i', \tag{6}$$

where ρ is the density of the sample. On the basis of the one-dimensional (1D) elastic equation, the bulk modulus K is derived as follows, by calculating the ratio of the stress σ_i' to strain ε_i':

$$K = \frac{|\sigma_i'|}{|\varepsilon_i'|}. \tag{7}$$

Actually, since the laser Doppler measurement in Fig. 1 is conducted at only one point on the surface boundary of the sample, the above-mentioned strain $|\varepsilon_i'|$ is approximated as follows, by using the simultaneously measured sample thickness l:

$$|\varepsilon_i'| = \frac{|u_i'|}{l}. \tag{8}$$

This processing corresponds to the calculation of the average strain in the inside of a sample, when it is assumed that the displacement at the bottom boundary of the sample is zero.

When the stress $|\sigma_i'|$ is constant and the sample has the thickness in which the influence of attenuation is negligible, the inverse of strain (IS), $1/|\varepsilon_i'|$, is proportional to the bulk modulus K. The bulk modulus K can be expressed as $K = E/[3(1-2\nu)]$, by using Young's modulus E and Poisson's ratio ν in the isotropic and linear elastic body. Therefore, since the IS has the potential to evaluate elasticity, the IS is used as the elasticity evaluation index in this paper. In the following sections, the feasibility of the proposed method for regenerating cartilage samples is investigated.

3. Measurement System

Figure 2 shows the measurement system used in this study. A cylindrical sample tank contained phosphate buffered saline (PBS) whose temperature was kept at 20.0 °C. In the sample tank, a circular urethane-based acoustic coupler (Takiron STD112) with a thickness of 10 mm and a diameter of 20 mm was put on the surface of an ultrasound transducer with a planar aperture, a center frequency of 1 MHz, and a circular element with a diameter of 6 mm (GE Sensing and Inspection Tech. 221-340), and an extracted regenerating cartilage sample was put on the acoustic coupler. Here, the density and sound speed of the acoustic coupler were 1.01×10^3 kg/m^3 and 1519 m/s, respectively, where the density was determined by measuring the increment in the volume of water when immersing the coupler in the water and the weight of the coupler, and the sound speed was determined by measuring the round-trip propagation time of multiple echoes through the inside of the coupler and the thickness of the coupler. A laser Doppler vibrometer (LDV; Graphtec AT0023 and AT3700) with a spot diameter of 20 μm and frequency ranges up to 10 MHz was set up 30 cm away from the cartilage sample surface. The spot of LDV was also positioned on the central axis of the acoustic field, by irradiating a visible red laser beam (wavelength: 632.8 nm) on the aperture center of the ultrasound transducer before putting the coupler on the transducer. On the basis of such settings, since the central axis of the acoustic field can

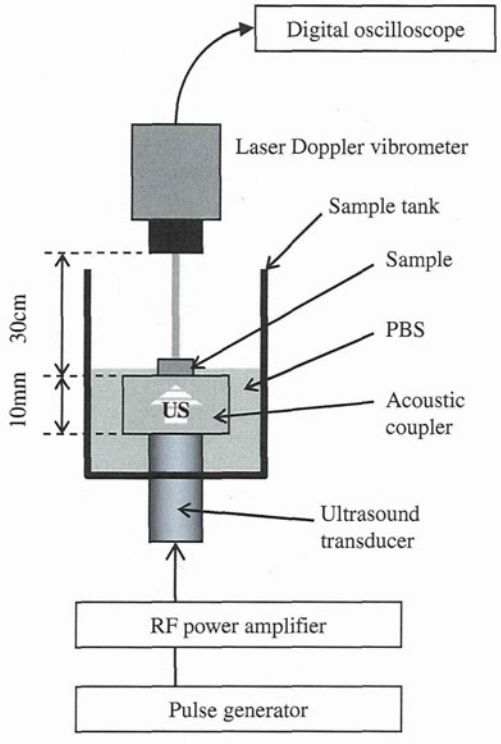

Fig. 2. Setup for laser Doppler measurement of ultrasound particle velocity.

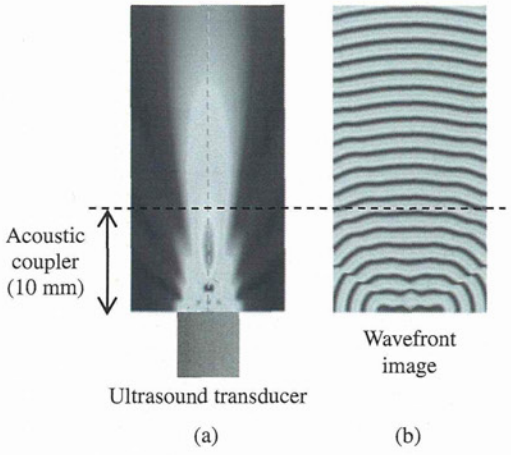

Fig. 3. Simulated acoustic field in the experimental setup: (a) acoustic field and (b) wavefront distribution.

be identified by observing the position of the visible laser spot, the central axis of the acoustic field can be easily placed on the center position of the sample.

On the other hand, the thickness of the acoustic coupler was determined by acoustic field simulation using the Rayleigh formula in a homogeneous medium. In this simulation, the acoustic field is calculated from the surface integral of spherical wave radiation on the above transducer aperture. Since this study considered only the small region of acoustic field around the central axis, no generations of shear wave and surface acoustic wave were considered in this simulation. Figures 3(a) and 3(b) show the calculated acoustic field and wavefront distribution obtained by the phase calculation. In Fig. 3(a), a field more distant than 10 mm from the surface of ultrasound transducer is a far field. In the far field, although the wavefront is uniform along the lateral direction, it is predicted that the stress is not uniform along the lateral direction and exhibits a maximum value on the central axis. However, from the result of this simulation, the variation of amplitude along the lateral direction to the maximum amplitude on the central axis at a depth of 10 mm was 0.002% within a spot diameter of 20 μm in the LDV. Therefore, in this paper, it is assumed that the plane wave approximation is valid within the spot diameter of the LDV around the central axis of a far field.

After finishing the above setup, a pulsed-wave ultrasound with five cycles was irradiated to the bottom of the cartilage sample via the acoustic coupler. The applied voltage to the ultrasound transducer was 450 V_{pp} and was maintained constant. This acoustic output which arises from this applied voltage generates the particle displacement of 0.46 μm on the surface of the acoustic coupler, which was obtained by the following root mean square (RMS) calculation for the particle displacement waveform on the surface of the acoustic coupler. Then, the LDV was used to measure the ultrasound particle velocity on the surface of the cartilage sample, and the particle velocity waveforms were recorded using a digital oscilloscope (LeCroy WS454VL) at a sampling frequency of 500 MHz. After recording the data, the particle velocity waveform is converted to the particle displacement waveform by temporal integration. Then, $|u_i'|$ in eq. (8) is attained by calculating the RMS of the particle displacement waveform. The calculation of RMS is also effective for obtaining a high signal-to-noise ratio. At the same time, the thickness of the sample, l in eq. (8), was also measured using a laser thickness indicator (Keyence LK-G35). Finally, the IS, that is, $1/|\varepsilon_i'|$, was calculated using eq. (8), and the elasticity of the regenerating cartilage sample was evaluated using the IS.

The obtained IS was compared with the Young's modulus measured by the static compression test. After IS measurement, the static compression test was conducted using an Instron-type universal testing machine (A&D UTM-10T). The sample was quasistatically compressed by a plate-type indenter with a diameter of 10 mm at a constant crosshead speed of 2 mm/min, and at the same time, the compression forces were measured using a load cell (rating capacity of 1 kg, resolution of 0.02% of rating capacity). Stress and strain were calculated from the measured forces and the dimensions of the sample, and then the Young's modulus of the sample was calculated using the ratio of stress to strain. Here, while the IS reflects the bulk modulus, the Young's modulus is measured in the the static compression test. However, under the assumption that Poisson's ratio is constant, the bulk modulus is proportional to the Young's modulus. Therefore, in the following experiments, the Young's modulus was referred to for verifying the capability of IS in the elasticity evaluation.

4. Phantom Experiment

To investigate the feasibility of this method for distinguishing the elasticity of a sample, three homogeneous phantoms with different elasticities (0.05, 0.1, 0.2 MPa as Young's

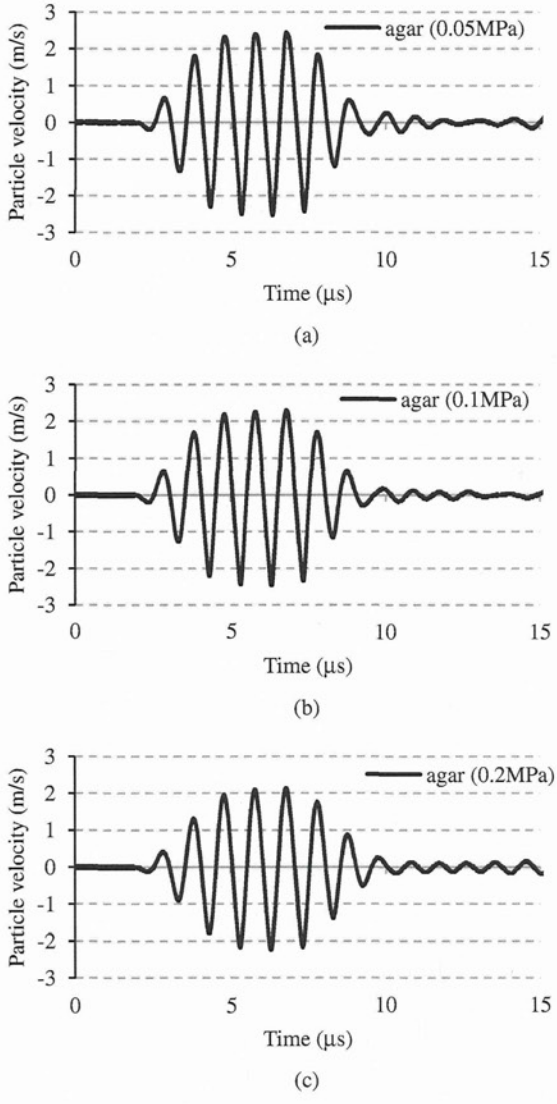

Fig. 4. Examples of particle velocity waveforms on the surface of agar-based phantoms: (a) 0.05, (b) 0.1, and (c) 0.2 MPa.

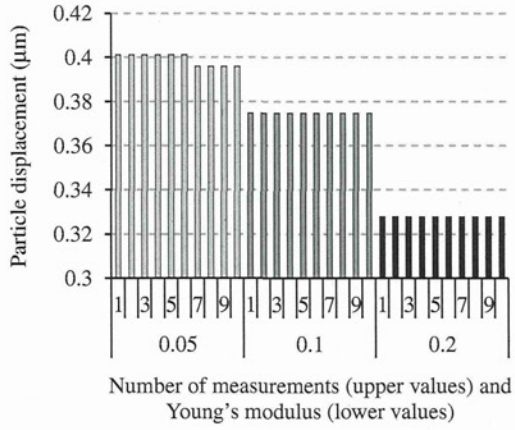

Fig. 5. Particle displacement values on the surface of agar-based phantoms.

modulus) and a constant size (each side of 10 mm, thickness of 5 mm) were formed by changing the weight concentration of agar powder. The Young's moduli of these phantoms were measured by the static compression test described in §3. Since the weight concentration of agar powder correlates with its elasticity, the three phantoms simulate the temporal elasticity change according to the maturity of the regenerating cartilage sample. Here, the densities of the agar-based phantoms with Young's moduli of 0.05, 0.1, and 0.2 MPa were 1.01×10^3, 1.02×10^3, and 1.02×10^3 kg/m^3, respectively. Likewise, the sound speeds of the agar-based phantoms with Young's moduli of 0.05, 0.1, and 0.2 MPa were 1520, 1532, and 1556 m/s, respectively. These densities and sound speeds were measured by using the density and sound speed measurement methods of the acoustic coupler as described in §3.

Each phantom was put on the acoustic coupler, and the laser spot was placed at the center position of the phantom surface. As mentioned in §3, since the magnitude of stress is not uniform along the lateral direction and exhibits a maximum value on the central axis, it is predicted that the particle velocity measured by the LDV is affected by the spot positioning. However, in this study, the spot is always placed on the central axis of the acoustic field, and the plane wave approximation is valid within the spot diameter of the LDV around the central axis of the far field. Therefore, in a homogeneous phantom, the particle velocity measurement is not affected by the stress distribution along the lateral direction.

Figure 4 shows examples of particle velocity waveforms measured by the LDV. As the elasticity of the agar-based phantom increases, a slight decrease in waveform amplitude can be observed. Figure 5 shows the RMS values of particle displacement waveforms on the surface of each phantom. The horizontal axis indicates the number of measurements on the same surface point of each phantom (upper values) and the Young's modulus variation (lower values). Since the thickness of each phantom was constant, the displacement decreased with the increase in elasticity. In addition, this result shows that the reproducibility of the measured results is good. Figure 6 shows a comparison between the IS obtained by the method described in §2 and the Young's modulus measured by the static compression test. The tendency of IS coincided well with that of the Young's modulus measured by the static compression test. That is, this method is capable of evaluating sample elasticity.

5. Regenerating Cartilage Sample Measurements

In vitro measurements using the regenerating cartilage samples (Fig. 7), which were extracted from beagles in approved animal experiments, were conducted by using the above-mentioned system. Autologous auricular cartilage cells of the beagle were transfused into a poly(L-lactic acid) (PLLA) scaffold and cultured during a certain period of time. The scaffolds with the cultured cells were transplanted subcutaneously in the same beagle and extracted after 2 months. Figure 7(a) shows photographs of regenerating cartilage samples extracted after culturing for 1 week (1wk), 2 weeks (2wk), and 3 weeks (3wk). Here, "control" means the cartilage sample regenerated using only the scaffold without any cells. Figure 7(b) shows optical photomicrographs of toluidine blue stain for the samples

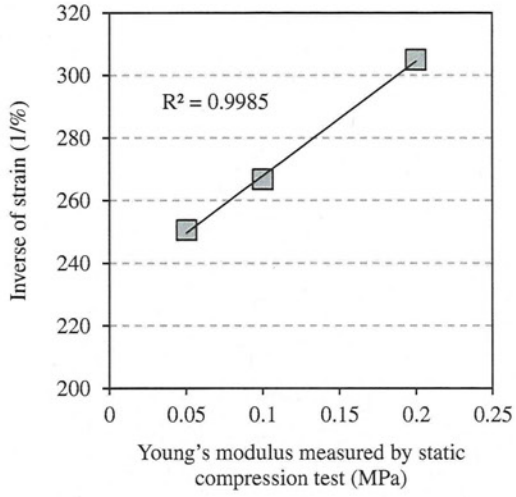

Fig. 6. Comparison between inverse of strain (IS) and Young's modulus measured by the static compression test.

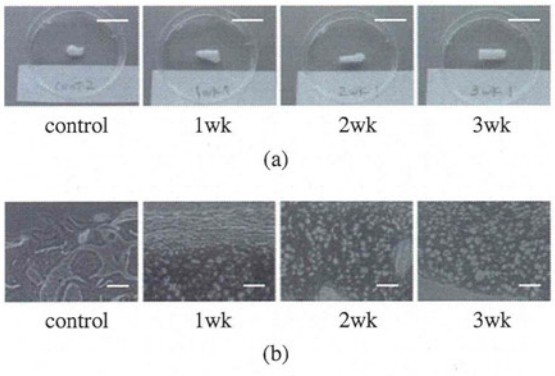

Fig. 7. Regenerating cartilage samples extracted from beagles: (a) photographs of regenerating cartilage samples extracted after culturing for 1 week (1wk), 2 weeks (2wk), and 3 weeks (3wk), and "control" means the cartilage sample regenerated using only the scaffold without any cells. Each bar indicates 10 mm length. (b) optical photomicrographs of toluidine blue stain for the samples shown in (a). Each bar indicates 100 μm length.

shown in Fig. 7(a). Here, only the density and sound speed of the native auricular cartilage tissue of the beagle (not shown here) were measurable, because the size of that native cartilage tissue sample was sufficient to measure the density and sound speed by using the density and sound speed measurement methods of the acoustic coupler as described in §3. As the result, the density and sound speed were $1.02 \times 10^3\,\mathrm{kg/m^3}$ and 1599 m/s, respectively. It can be predicted that the acoustic properties of regenerating cartilage tissue become gradually close to those of native cartilage tissue. Therefore, the acoustic impedance determined using the measured density and sound speed is regarded as the maximum acoustic impedance that the regenerating cartilage tissue used in this study attains. On the other hand, as the minimum acoustic impedance, it is reasonable to assume the acoustic impedance of water because the water content of cartilage tissue is high and the acoustic impedance of cartilage tissue is higher than that of water. Therefore, when the density and sound speed of water are assumed to be $1.00 \times 10^3\,\mathrm{kg/m^3}$ and 1500 m/s, respectively, the acoustic impedance of regenerating cartilage tissue used in this study can vary within 1.5×10^6 to $1.64 \times 10^6\,\mathrm{kg/(m^2 \cdot s)}$. The extracted cartilage sample (width of 5 mm, thickness of 1 mm) was placed on the acoustic coupler, and the elasticity was evaluated using IS, as well as the above phantom measurements. The LDV spot was also placed on the center position of the regenerating cartilage sample surface. Since the wavelength in the regenerating cartilage sample is predicted to be about 1.6 mm, which is larger than the thickness of the sample, the obtained IS corresponds to the average value along the thickness direction.

Figure 8 shows examples of particle velocity waveforms on the regenerating cartilage sample surface measured using the LDV. As the culture period increases, a slight decrease in the maximum amplitude in the primary waveform located at 5 to 13 μs was observed. Considering the thicknesses of the coupler and sample, the smaller-amplitude waves at approximately 15 μs in Figs. 8(a)–8(c) are the reflection waves in the inside of the coupler and sample, are not the progressive waves intended for elasticity evaluation. Therefore, the RMS calculations for obtaining IS were conducted in the above primary waveform within a constant duration considering the pulse width, and these smaller-amplitude waveforms are not included in the RMS calculations.

Figure 9 shows the IS of regenerating cartilage samples according to the culture periods of 1, 2, and 3 weeks. Again, "control" means the cartilage sample regenerated using only the scaffold without any cells. At the measuring position in this experiment, the IS values of regenerating cartilage samples increased with an increase in the culture period. In addition, these IS values also increased with an increase in the Young's modulus of regenerating cartilage samples measured by the static compression test (for example, 2.05 MPa for 1 week, 2.2 MPa for 2 weeks and 2.5 MPa for 3 weeks). Although additional verifications using many regenerating cartilage samples are required for concluding the relationship between the maturity and elasticity of the regenerating cartilage, at least the above results imply that the IS discriminates the differences in elasticity of the regenerating cartilage and that the IS predicts that longer culture periods induce a tendency to regenerate stiffer cartilage tissues.

6. Discussion

This method assumes that only the plane progressive wave propagates inside the homogeneous cartilage sample, the sample has the thickness in which the influence of attenuation is negligible, and the stress inside the sample is constant. Actually, however, not only the incident wave but also the reflected wave from the surface boundary of the sample exists in the inside of the sample. In addition, only the applied stress at the boundary between the coupler and cartilage sample is constant. Since the incident wave penetrating inside of the sample is affected by variation of the acoustic impedance of the sample, the stress inside the sample is affected by the acoustic impedance. Here, we discuss the influence of acoustic impedance variation of the sample in the elasticity evaluation, on the basis of a three layer model including a coupler layer, cartilage sample layer, and surrounding air, as shown in Fig. 10.

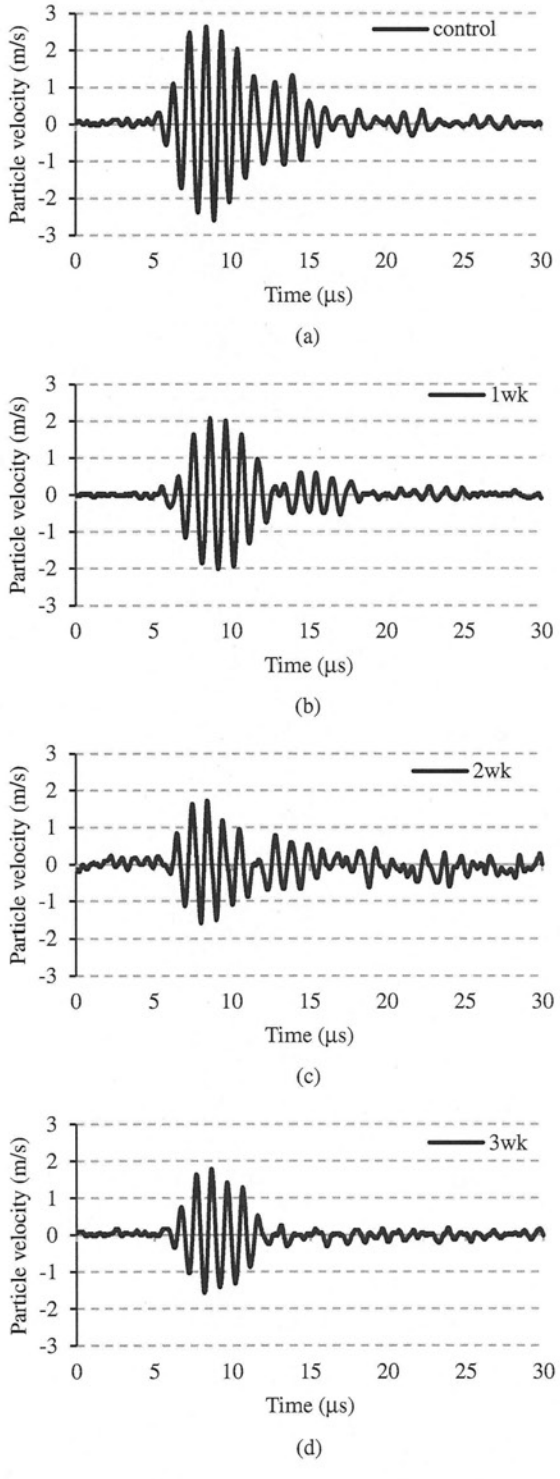

Fig. 8. Examples of particle velocity waveforms on the surface of regenerating cartilage samples: (a) control, (b) 1 week (1wk), (c) 2 weeks (2wk), and (d) 3 weeks (3wk).

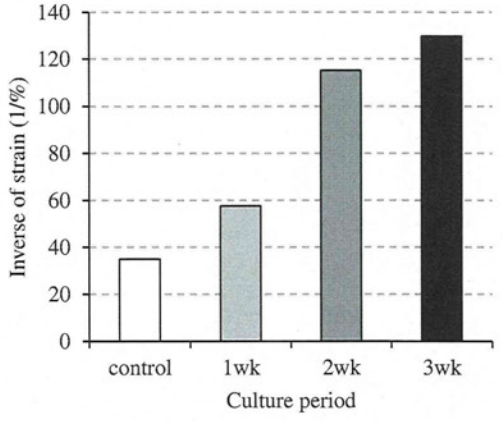

Fig. 9. Results of inverse of strain (IS) according to the culture periods in the regenerating cartilage sample.

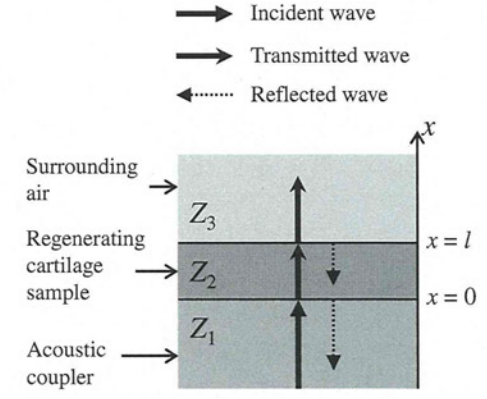

Fig. 10. Three-layer model for investigating the influence of acoustic impedance variation of samples in the proposed elasticity evaluation.

In Fig. 10, the coupler layer includes an incident wave and a reflected wave from the boundary of $x = 0$, the cartilage sample layer includes a transmitted wave from the boundary of $x = 0$ and a reflected wave from the boundary of $x = l$, and the surrounding air includes only the transmitted wave from the boundary of $x = l$. The LDV measures particle velocity at $x = l$, and this particle velocity is equivalent to the particle velocity inside the homogeneous sample, as described in §2. The effective value v' of particle velocity at $x = l$ is expressed as follows, by using the particle velocity component v'_i of the transmitted wave and the particle velocity component v'_r of the reflected wave inside the regenerating cartilage sample:

$$\begin{aligned} v' &= v'_i + v'_r \\ &= jk(\phi'_i - \phi'_r), \end{aligned} \tag{9}$$

where ϕ'_i and ϕ'_r are the velocity potential components of the transmitted and reflected waves inside the regenerating cartilage sample, respectively. The effective value v'_i is the same as that shown in eq. (2). From the particle velocity, the strain ε' at $x = l$ is derived as follows, by using the strain component ε'_i induced by the transmitted wave and the strain component ε'_r induced by the reflected wave inside the regenerating cartilage sample:

$$\begin{aligned} \varepsilon' &= \varepsilon'_i + \varepsilon'_r \\ &= -j\frac{k}{c}(\phi'_i + \phi'_r), \end{aligned} \tag{10}$$

where ε'_i is the same as that shown in eq. (5). In the actual situation, however, $1/|\varepsilon'|$ is evaluated as IS. In this discussion, $1/|\varepsilon'|$ is referred to as the apparent inverse of strain (AIS) and is distinguished from the IS. Similarly, the

stress σ' at $x = l$ on the side of the cartilage sample is derived as follows, by using the stress component σ'_i induced by the transmitted wave and the stress component σ'_r induced by the reflected wave inside the regenerating cartilage sample:

$$\sigma' = \sigma'_i + \sigma'_r = j\omega_0\rho(\phi'_i + \phi'_r), \quad (11)$$

where σ'_i is the same as that shown in eq. (6). On the other hand, since only the transmitted wave exists in the surrounding air, the stress σ'_{3i} at $x = l$ on the side of the air is derived as follows:

$$\sigma'_{3i} = j\omega_0\rho_3\phi'_{3i}, \quad (12)$$

where ρ_3 is the density of air and ϕ'_{3i} is the velocity potential component of the transmitted wave in the air. These stresses are continuous at $x = l$ as follows:

$$\sigma' = \sigma'_{3i}. \quad (13)$$

Moreover, the stress σ'_{1i} at $x = 0$ induced by the incident wave inside the coupler is derived as follows:

$$\sigma'_{1i} = j\omega_0\rho_1\phi'_{1i}, \quad (14)$$

where ρ_1 is the density of the coupler and ϕ'_{1i} is the velocity potential component of the incident wave in the coupler. When σ'_i and ε'_i in eq. (7) are replaced by σ'_{1i} and ε', respectively, AIS is derived as follows, by using eqs. (10)–(14):

$$\frac{1}{|\varepsilon'|} = \frac{1}{|\sigma'_{1i}|}\frac{K}{|T_p|}, \quad (15)$$

where $|T_p|$ is the transmission coefficient of the incident wave inside the coupler, which is defined by the ratio of σ'_{3i} to σ'_{1i}. $|T_p|$ is derived as follows, by using the acoustic impedances Z_1, Z_2, and Z_3 in the layers shown in Fig. 10:

$$|T_p| = \frac{2}{\sqrt{\left(1+\frac{Z_1}{Z_3}\right)^2\cos^2(kl) + \left(\frac{Z_2}{Z_3}+\frac{Z_1}{Z_2}\right)^2\sin^2(kl)}}. \quad (16)$$

Since only the incident wave inside the coupler is constant, the stress σ'_{1i} at $x = 0$ induced by the foremen-tioned incident wave is also constant. Therefore, AIS is proportional to $K/|T_p|$ and is affected by the acoustic impedance variation of the cartilage sample.

To evaluate the influence of $|T_p|$, a calculated result of $K/|T_p|$ to true K is shown in Fig. 11. Here, the horizontal and vertical lines indicate the true K and $K/|T_p|$, respectively. The vertical line corresponds to the AIS. In particular, $K/|T_p|$ was calculated by substituting the acoustic impedance values of the coupler and air ($Z_1 = 1.01 \times 10^3$ [kg/m^3] $\times$ 1519 [m/s] $= 1.53 \times 10^6$ [kg/(m^2·s)], $Z_3 = 1.2$ [kg/m^3] $\times$ 343 [m/s] $= 412$ [kg/(m^2·s)]), frequency (1 MHz), and sample thickness l into eq. (16), and changing the acoustic impedance Z_2 of the sample within the realistic range. The thick solid line in Fig. 11 indicates the relationship between K and $K/|T_p|$ in the agar-based phantoms, when the thickness of 5 mm, the density within the range of 1.01×10^3 to 1.02×10^3 kg/m^3, and the sound speed within the range of 1510 to 1580 m/s are substituted into eq. (16). Here, it was assumed that $K = \rho c^2$. The

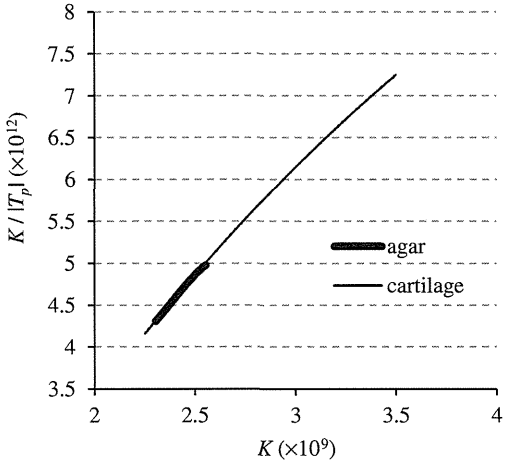

Fig. 11. Comparison between true bulk modulus (horizontal line) and bulk modulus affected by the acoustic impedance variation of samples (vertical line).

relationship between K and $K/|T_p|$ is almost linear. In addition, the thin solid line in Fig. 11 indicates the relationship between K and $K/|T_p|$ in the cartilage samples, when the thickness of 1 mm, the density within the range of 1.00×10^3 to 1.20×10^3 kg/m^3, and the sound speed within the range of 1500 to 1700 m/s are substituted into eq. (16). This acoustic impedance range is wider than that predicted in §5, and the density and sound speed are appropriate for typical cartilage tissues. Again, the relationship between K and $K/|T_p|$ is almost linear. Since the IS is proportional to K and the AIS is also proportional to $K/|T_p|$, consequently, the AIS is proportional to K and IS. Therefore, these relationships imply that AIS can be referred to as IS, and the obtained AIS is usable for elasticity evaluation. Actually, since the experimental results also showed that the relationship between IS and Young's modulus was linear, the feasibility of the proposed method for elasticity evaluation was verified theoretically and experimentally. On the basis of this linear relationship, some appropriate calibrations might enable the quantitative evaluation of elasticity.

On the other hand, eq. (16) includes sinusoidal components (cos and sin). These components are affected by the thickness of the sample, the sound speed of the sample, and the used frequency. However, as shown in Fig. 11, no significant oscillations due to sinusoidal components appear in response to changes in the sound speed of the sample. Therefore, it is important that the appropriate frequency and sample thickness are selected so that the linear relationship between IS and K is maintained within the range of the required elastic modulus and the influence of attenuation is reduced. Consequently, the above discussion showed that the frequency of 1 MHz and sample thickness of 1 or 5 mm in the experiments were appropriate for the elasticity evaluation of a cartilage sample.

7. Conclusions

The feasibility of the proposed method was suggested through the phantom and regenerating cartilage sample measurements. Results of experimental and theoretical investigations showed that the IS measured in the proposed

method enabled elasticity evaluations. In a future work, elasticity imaging by scanning the ultrasound beam and the LDV spot simultaneously will be interesting. At the same time, the effectiveness of the proposed method must be verified through measurements of a number of regenerating cartilage samples. Moreover, strategies for *in vivo* measurement of regenerating cartilage must also be investigated.

Acknowledgments

This work was supported by a Research and Development of Three-dimensional Complex Organ Structures, NEDO, Japan, and a Grant-in-Aid for Scientific Research A (22240063) from the Japan Society for the Promotion of Science. We appreciate Dr. Hoshi of the University of Tokyo who supplied us with the valuable regenerating cartilage samples in animal experiments.

1) T. Otani, I. Mano, T. Tsujimoto, T. Yamamoto, R. Teshima, and H. Naka: Jpn. J. Appl. Phys. **48** (2009) 07GK05.
2) Y. Yaoi, K. Yamamoto, T. Nakatsuji, T. Yanagitani, M. Matsukawa, K. Yamazaki, and A. Nagano: Jpn. J. Appl. Phys. **48** (2009) 07GK06.
3) A. Hosokawa: Jpn. J. Appl. Phys. **48** (2009) 07GK07.
4) M. Ohno, N. Ikeda, K. Ohira, and Y. Ogawa: Jpn. J. Appl. Phys. **48** (2010) 07HF27.
5) S. Hasegawa, Y. Nagatani, K. Mizuno, and M. Matsukawa: Jpn. J. Appl. Phys. **48** (2010) 07HF28.
6) F. Rupin, A. Saïed, D. Dalmas, F. Peyrin, S. Haupert, K. Raum, E. Barthel, G. Boivin, and P. Laugier: Jpn. J. Appl. Phys. **48** (2009) 07GK01.
7) C. G. Armstrong and V. C. Mow: J. Bone Joint Surg. **64** (1982) 88.
8) J. S. Wayne, K. A. Kraft, K. J. Shields, C. Yin, J. R. Owen, and D. G. Disler: Radiology **228** (2003) 493.
9) L. P. Li, W. Herzog, R. K. Korhonen, and J. S. Jurvelin: Med. Eng. Phys. **27** (2005) 51.
10) L. P. Li, R. K. Korhonen, J. Iivarinen, J. S. Jurvelin, and W. Herzog: Med. Eng. Phys. **30** (2008) 182.
11) P. C. Lin, D. A. Reiter, and R. G. Spencer: J. Magn. Reson. **201** (2009) 61.
12) M. J. Nissi, J. Rieppo, J. Töyräs, M. S. Laasanen, I. Kiviranta, M. T. Nieminen, and J. S. Jurvelin: Osteoarthritis Cartilage **15** (2007) 1141.
13) V. Mlynárik, I. Sulzbacher, M. Bittsanský, R. Fuiko, and S. Trattnig: J. Magn. Resonance Imaging **17** (2003) 440.
14) Q. Wang and Y. P. Zheng: Ultrason. Med. Biol. **35** (2009) 1535.
15) E. H. Chiang, T. J. Laing, C. R. Meyer, J. L. Boes, J. M. Rubin, and R. S. Adler: Ultrason. Med. Biol. **23** (1997) 205.
16) M. H. Lu, Y. P. Zheng, and Q. H. Huang: Ultrason. Med. Biol. **31** (2005) 817.
17) S. Z. Wang, Y. P. Huang, S. Saarakkala, and Y. P. Zheng: Ultrason. Med. Biol. **36** (2010) 512.
18) H. J. Nieminen, P. Julkunen, J. Töyräs, and J. S. Jurvelin: Ultrason. Med. Biol. **33** (2007) 1755.
19) J. K. F. Suh, I. Youn, and F. H. Fu: J. Biomech. **34** (2001) 1347.
20) J. Töyräs, M. S. Laasanen, S. Saarakkala, M. J. Lammi, J. Rieppo, J. Kurkijärvi, R. Lappalainen, and J. S. Jurvelin: Ultrason. Med. Biol. **29** (2003) 447.
21) S. G. Patil, Y. P. Zheng, and X. Chen: Ultrason. Med. Biol. **36** (2010) 1345.
22) H. J. Nieminen, S. Saarakkala, M. S. Laasanen, J. Hirvonen, J. S. Jurvelin, and J. Töyräs: Ultrason. Med. Biol. **30** (2004) 493.
23) S. Saarakkala, M. S. Laasanen, J. S. Jurvelin, K. Törrönen, M. J. Lammi, R. Lappalainen, and J. Töyräs: Osteoarthritis Cartilage **11** (2003) 697.
24) P. Kiviranta, E. Lammentausta, J. Töyräs, I. Kiviranta, and J. S. Jurvelin: Osteoarthritis Cartilage **16** (2008) 796.
25) A. S. Aula, J. Töyräs, V. Tiitu, and J. S. Jurvelin: Osteoarthritis Cartilage **18** (2010) 1570.
26) B. Pellaumail, A. Watrin, D. Loeuille, P. Netter, G. Berger, P. Laugier, and A. Saïed: Osteoarthritis Cartilage **10** (2002) 535.
27) S. Saarakkala, S. Z. Wang, Y. P. Huang, J. S. Jurvelin, and Y. P. Zheng: Ultrason. Med. Biol. **37** (2011) 112.
28) K. Hattori, K. Mori, T. Habata, Y. Takakura, and K. Ikeuchi: Clin. Biomech. **18** (2003) 553.
29) M. Fortin, M. D. Buschmann, M. J. Bertrand, F. S. Foster, and J. Ophir: J. Biomech. **36** (2003) 443.
30) Y. P. Zheng, H. J. Niu, F. T. A. Mak, and Y. P. Huang: J. Biomech. **38** (2005) 1830.
31) M. S. Laasanen, J. Töyräs, A. Vasara, S. Saarakkala, M. M. Hyttinen, I. Kiviranta, and J. S. Jurvelin: Osteoarthritis Cartilage **14** (2006) 258.
32) S. Saarakkala, J. Töyräs, J. Hirvonen, M. S. Laasanen, R. Lappalainen, and J. S. Jurvelin: Ultrason. Med. Biol. **30** (2004) 783.
33) C. Y. Tsai, C. L. Lee, C. Y. Chai, C. H. Chen, J. Y. Su, H. T. Huang, and M. H. Huang: Osteoarthritis Cartilage **15** (2007) 245.
34) J. Töyräs, T. Lyyra-Laitinen, M. Niinimaki, R. Lindgren, M. T. Nieminen, I. Kiviranta, and J. S. Jurvelin: J. Biomech. **34** (2001) 251.
35) L. Mancarella, M. Magnani, O. Addimanda, E. Pignotti, S. Galletti, and R. Meliconi: Osteoarthritis Cartilage **18** (2010) 1263.
36) T. Virén, S. Saarakkala, E. Kaleva, H. J. Nieminen, J. S. Jurvelin, and J. Töyräs: Ultrason. Med. Biol. **35** (2009) 1546.
37) N. Nitta, K. Homma, M. Misawa, K. Hoshi, S. Bu, and T. Shiina: Proc. IEEE Int. Ultrasonics Symp., 2010, p. 1400.
38) Y. Tanaka, Y. Saijo, Y. Fujihara, H. Yamaoka, S. Nishizawa, S. Nagata, T. Ogasawara, Y. Asawa, T. Takato, and K. Hoshi: J. Biosci. Bioeng. **113** (2012) 252.
39) V. C. Mow, S. C. Kuei, W. M. Lai, and C. G. Armstrong: J. Biomech. Eng. **102** (1980) 73.